

# An Alaska-Aleutian subduction zone interface earthquake recurrence model from geology and geodesy

Rich Briggs<sup>1</sup>

<sup>1</sup>Affiliation not available

December 10, 2023

Rich Briggs<sup>1</sup>, Robert C. Witter<sup>2</sup>, Jeffrey T. Freymueller<sup>3</sup>, Peter M. Powers<sup>1</sup>, Peter J. Haeussler<sup>2</sup>, Stephanie L. Ross<sup>4</sup>, Tina Dura<sup>5</sup>, Simon E. Engelhart<sup>6</sup>, Richard D. Koehler<sup>7</sup>, Hong Kie Thio<sup>8</sup>

<sup>1</sup> U.S. Geological Survey, Geological Hazards Science Center, Golden, CO, USA

<sup>2</sup> U.S. Geological Survey, Alaska Science Center, Anchorage, AK, USA

<sup>3</sup> Department of Earth and Environmental Sciences, Michigan State University, East Lansing, MI, USA

<sup>4</sup> Pacific Coastal and Marine Science Center, US Geological Survey, Moffett Field, CA, USA

<sup>5</sup>Department of Geosciences, Virginia Tech, Blacksburg, VA, USA

<sup>6</sup>Department of Geography, Durham University, Durham, UK

<sup>7</sup>Nevada Bureau of Mines and Geology, University of Nevada, Reno, Reno, NV, USA

<sup>8</sup> AECOM, Los Angeles, CA, USA

Corresponding author: Rich Briggs (rbriggs@usgs.gov)

## Key Points:

- We present earthquake recurrence estimates from geologic and geodetic data for the Alaska-Aleutian subduction zone
- Recurrence estimates provide constraints for seismic hazard models
- The recurrence estimates indicate that the rates of  $M_w$  [?] 8 ruptures are higher than previously inferred west of Kodiak Island

NOTE: This paper is in press at AGU Books and has USGS BAO approval for publication (IP-152990). The final version may contain copy edits.

## Abstract

Seismic hazard models rely on earthquake recurrence estimates, but histories of earthquakes with long recurrence intervals can be difficult to derive for subduction zones from historical seismicity alone. Here we present an earthquake recurrence model for the subduction interface of the Alaska-Aleutian subduction zone based on geodetic and paleoseismic data. To capture variations in rupture behavior along strike, we define fault sections based on geodetic coupling, prehistoric earthquake and tsunami recurrence, historical ruptures, and geologic and geophysical structure. From east to west along the subduction zone, several key findings guide construction of the recurrence model. The Yakataga section exhibits a complex interplay

of strain accumulation along the Yakutat plate interface and upper-plate faulting. In the 1964  $M_w$  9.2 rupture area, which spans four fault sections, recurrence rates for section participation in presumed great ( $M_w$  8.5+) events vary from  $\sim 600$  years (Prince William Sound section) to  $\sim 380$  years (Kodiak section), geodetic character varies substantially along strike, and geologic evidence indicates rupture patches vary in space and time. Westward along the Semidi section, recurrence of large, tsunamigenic ruptures are far more frequent ( $\sim 220$  years) based on geologic and geodetic data than previously assumed. The seismic potential of the Shumagin section, an area of low coupling, remains enigmatic despite a large ( $M_w$  7.8) rupture in 2020. The neighboring Sanak section, which is nearly freely slipping, appears to produce large events every  $\sim 1,000$  years, most recently in 1946 ( $M_w$  8.6). Prehistoric tsunami data indicate that large rupture recurrence in the Fox Islands is  $\sim 210$  years. Paleoseismic data is lacking west of the Fox Islands, so rupture rates along the western 1900 km of the subduction interface to Komandorski rely on geodetic constraints. Simple recurrence estimates from geodetic data suggest that rates for  $M_w$  8+ earthquakes are higher than previously assumed from seismicity alone west of the Fox Islands.

## 1 Introduction

Earthquake rupture forecasts rely in part on geologic deformation models that combine fault geometries and long-term fault slip rates (Field et al., 2014; Hatem et al., 2022). For subduction interfaces, deformation models can be difficult to construct because simple notions of fault slip rates do not apply to subduction systems. This is because geodetic coupling varies along strike and downdip (Chlieh et al., 2008; Freymueller & Beavan, 1999; Lay et al., 2012; Pacheco et al., 1993; Scholz & Campos, 2012; Wang, 1995) and strain release along subduction interfaces can be complicated by complex, overlapping patterns of aseismic, coseismic, and postseismic slip and upper-plate structures such as splay faults (Barnhart et al., 2016; Liberty et al., 2013). Because aseismic slip is nearly ubiquitous in the subduction setting, fault slip rates are replaced by the concept of slip deficit rates, which represent the long-term plate convergence rate times the coupling coefficient along the subduction interface determined geodetically (Pacheco et al., 1993). The coupling coefficient ranges from 0 (or 0%) when the interface is fully decoupled and the interseismic (aseismic) slip rate is equal to the local plate convergence rate, to 1 (or 100%) when the interface is fully locked and the slip deficit rate equals the local plate convergence rate (Pacheco et al., 1993).

Recurrence estimates based on paleoseismic data are especially important in subduction zones because the return times of the largest subduction earthquakes greatly exceed the length of historical seismic catalogs and slip deficit rates are not easily converted to earthquake rates (Nelson et al., 2021; Satake & Atwater, 2007). Subduction paleoseismology provides estimates of earthquake recurrence from abrupt changes in relative sea level recorded by geologic archives, such as coastal marsh stratigraphy (Atwater, 1987) and coral microatolls (Taylor et al., 1987). Indirect proxies for subduction interface rupture include turbidites (Adams, 1990; Goldfinger et al., 2012) and tsunami inundation (Witter et al., 2016).

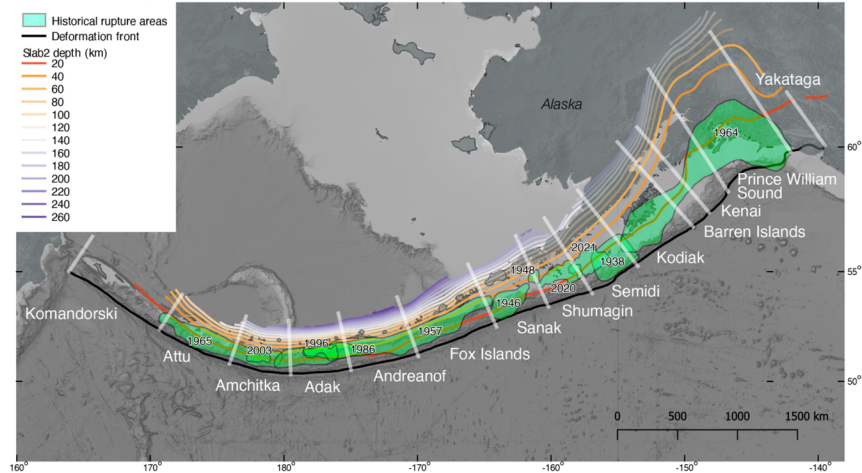


**Figure 1. Study area along the Alaska-Aleutian subduction zone (AASZ) showing the locations of fault sections and approximate historical rupture areas. For older events, rupture areas are inferred from aftershock zones (Tape and Lomax, 2022), and recent events are taken from fault rupture models (Freymueller et al., 2021; Tape & Lomax, 2022; Ye et al., 2022). Slab interface contours are from Hayes et al., 2018. Bathymetry and shaded relief from GEBCO Compilation Group (2023).**

The last update to the Alaska portion of the U. S. Geological Survey (USGS) National Seismic Hazard Model (NSHM) in 2007 used the best available information to define recurrence rates for seven fault sections along the subduction interface, primarily based on rupture areas of historical subduction earthquakes (Wesson et al., 2007). Maximum magnitudes were assigned to each fault section, and seismicity and limited paleoseismic data were used to estimate rupture recurrence (Wesson et al., 2007). At the time of the Wesson et al. (2007) update, paleoseismic and paleotsunami records extended westward only as far as Kodiak Island, and so seismicity rates exclusively were used west of Kodiak to approximate the recurrence of large ruptures. Geodetic data (Freymueller et al., 2008) were not incorporated in the 2007 update.

There have been several advances in the treatment of subduction zone hazard since the last update of the Alaska portion of the NSHM in 2007. In New Zealand, geodetic data were incorporated into the Hikurangi subduction interface model of Stirling et al. (2012), where rupture segments were defined based on the pattern of interseismic coupling, slow slip events, and historical seismicity and earthquake recurrence rates were inferred from plate convergence rates and coupling coefficients. The most recent New Zealand seismic hazard model also uses geodetic data, and leverages geologic data as a comparison, but not as a constraint, in the inversion for rupture rates (Coffey et al., 2022). By contrast, in Cascadia geodetic data are not used explicitly in recurrence models, but instead a rich onshore and offshore paleoseismic record is available to assign entire-zone and partial-rupture recurrence rates (Frankel et al., 2015). Recent global subduction zone recurrence models (Pagani et al., 2021) rely primarily on seismicity, especially where paleoseismic data are lacking.

Here, we construct a recurrence model for the Aleutian-Alaskan subduction zone using both geologic and geodetic data because these datasets provide different, but complementary, views of rupture behavior. Along the energetic coasts of Alaska, geologic data capture only the largest ruptures, generally with preserved evidence of vertical deformation above detection limits of  $> 0.2$  m (Hawkes et al., 2010; Shennan et al., 2016) or tsunami runup  $> 5$  m above the modern tidal range (Nelson et al., 2015; Witter et al., 2016, 2019). The geologic data also represent events that typically rupture multiple fault sections, which is demonstrated

by historical events and inferred for prehistoric earthquakes. The geodetic data is used to approximate strain accumulation and release by a single fault section. Thus, recurrence rates of ruptures inferred from geodetic data are necessarily shorter and the inferred earthquake magnitudes are smaller than events recorded by geology. Our goal is to provide parameters useful for seismic hazard analyses, such as for the next update of the USGS NSHM. The model focuses on subduction interface ruptures rather than outer rise, crustal, or intraslab events.

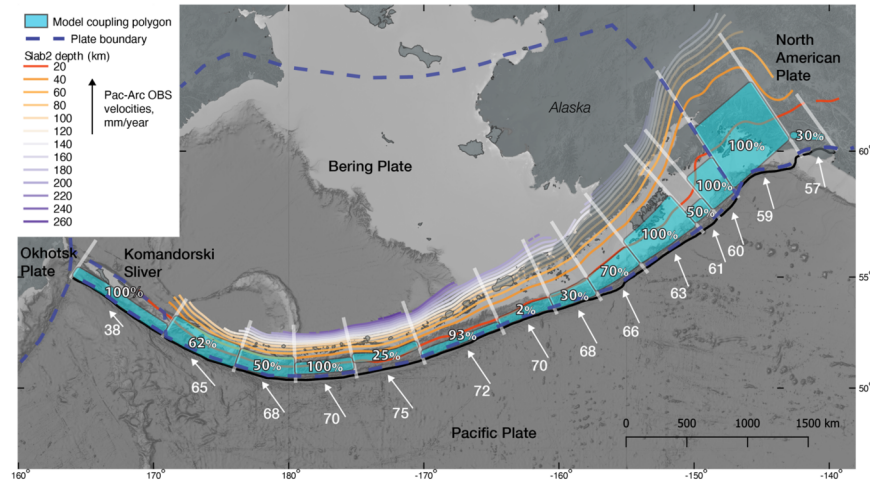


**Figure 2.** Overview of the geodetic coupling model and plate boundary context along the AASZ. Calculation of relative Pacific-Arc Observed (Pac-Arc OBS) velocities is described in the text. Sections as in Figure 1. Bering Plate boundary approximation from Mackey et al. (1997). Slab interface contours are from Hayes et al. (2018). Bathymetry and shaded relief from GEBCO Compilation Group (2023).

## 2 Methods and model inputs

### 2.1 Subduction interface geometry

Prior studies in Alaska have used a wide range of interface geometry models. The subduction interface geometry we use is simplified as a planar fit to the Slab2 interface model (Hayes et al., 2018) for use in hazard calculations. Generalization of the interface is reasonable because (1) at the shallow levels of the seismogenic interface where curvature is minimal, a plane is a reasonable approximation of the interface geometry; (2) the geodetic coupling models we use to calculate slip deficit rates assumed planar surfaces; and (3) geodetic polygons are not used to model seafloor deformation to generate tsunamis or predict the downdip extent of slip, but instead are used as a way to approximate moment accumulation.

The criteria above led us to approximate the potentially seismogenic plate interface as a series of rectangular elements, one for each section. The downdip width of the inferred seismogenic zone, combined with a slip deficit rate that is based on the relative plate motion multiplied by a coupling coefficient, gives a reasonable first-order approximation for the moment accumulation rate. As moment accumulation rate is the primary focus, we do not attempt to model spatial complexity at a smaller scale, but instead will average the slip deficit rate/coupling coefficient over the rectangle.

### 2.2 Subduction interface sections

We assign fault sections to broadly characterize earthquake recurrence and slip deficit rates along strike of the AASZ (Figure 1). Our selection of the term 'section' rather than 'segment' is intentional, as our analysis is

not meant to imply that each section is a fixed rupture segment. Previous segmentation models of the AASZ focused primarily on the historical pattern of ruptures, mainly inferred from aftershock zones (Davies et al., 1981; McCann et al., 1979; Sykes, 1971) (Figure 2). Here we define fault sections in part by historical and prehistoric rupture patches, but also geodetic data, geologic observations of land-level changes and tsunami recurrence, and structural observations. The sections are modified from those presented in the 2007 NSHM (Wesson et al., 2007) and many closely follow those defined by a coordinated effort by the National Tsunami Hazard Mitigation Program to devise tsunami source models for Alaska (Ross et al., 2023). The sections vary in length, ranging from from  $\sim 95$  km (Barren Islands section) to  $\sim 540$  km (Komandorski section) (Figure 1).

We defined sections based on observed along strike changes in criteria: changes in slip magnitude and/or depth range of slip in historical great earthquakes, changes in the interseismic slip deficit distribution (rate or spatial pattern) based on geodetic studies, or changes in earthquake recurrence estimated from paleo-earthquake or paleo-tsunami studies. We required along-strike changes in at least two of these quantities to define a section boundary. For example, the Barren Islands section, the shortest in our model, was defined (see Section 3 for details) based on a significant narrowing of the region of slip deficit observed in geodetic models (Suito & Freymueller, 2009; 2020), plus a corresponding narrowing of the region of slip in 1964 in the model of Ichinose et al. (2007).

The hazard modeling approach that will use our model values does not allow for variations in slip deficit with depth, but only updip and downdip limits of the seismogenic zone and a slip deficit rate/moment accumulation rate. The downdip limit is estimated from slip in known great earthquakes or from geodetic estimates. The updip limit is difficult to estimate because geodetic studies have very limited model resolution near the trench, and usually no more than one large or great earthquake has a known slip distribution. Even where earthquake slip distributions have been modeled, the extent of shallow slip may be poorly constrained without near-trench observations (e.g., Brooks et al., 2023). The tsunami record can demonstrate evidence of past slip to the trench (or near it), but if we lack clear evidence for the slip behavior of the megathrust at shallow depth, or if previous coupling models lack clear updip limits, we assume that the updip limit of slip deficit extends to the trench.

### 2.3 Geologic recurrence values

We summarize geologic recurrence values for each fault section in Table 1. Two primary types of recurrence data are depicted: recurrence inferred from land-level changes, and recurrence assumed from tsunami deposits. The sensitivity of both types of data to earthquake magnitude is unknown, and various combinations of slip, magnitude, and location likely influence land-level change and tsunami generation. Only the largest ( $M_w$  [?] 8.5) events may leave unambiguous records: for example, the  $M_w$  8.2 Chignik rupture generated a negligible near- and far-field tsunami and small ( $< 0.08$  m) vertical displacements (Elliott et al., 2022; Ye et al., 2022), less than the theoretical detection limit of 0.1- 0.2 m discussed by Shennan et al. (2016). Until more is known about the sensitivity of land-level change and tsunami recorders to earthquake rupture characteristics in the AASZ, we assume that the geologic data records earthquakes [?]  $M_w$  8.5.

Uncertainties are not reported in a standardized way for the geologic recurrence data we summarize here, so we use author-reported recurrence intervals and uncertainties. Where not supplied by the authors, we calculate the mean recurrence interval by dividing  $n-1$  events into the total closed interval (oldest event to most recent event) or  $n$  events into the total open interval (oldest event to present day) and assign uncertainty equal to the standard deviation of the mean recurrence value (Table 1). More complicated calculations are possible (Field et al., 2013) but are not yet warranted for the AASZ because of the relative lack of data, and the sometimes disparate approaches and assumptions used for event identification and subduction interface earthquake age estimates. We presume that recurrence calculations are standardized within any particular hazard model framework, and a logic tree approach will be used to propagate uncertainties in recurrence and paleo-event size for classic probabilistic seismic hazard analysis (National Research Council, 1997) or that recurrence values with standardized uncertainty will be used as a constraint in inversion-based PSHA (Field et al., 2020).

## 2.4 Geodetic recurrence values

Geodetic estimates of the slip deficit distribution along the AASZ have used a wide variety of modeling approaches, producing estimates of varying complexity. Some studies (e.g., Fournier & Freymueller (2007); Cross & Freymueller (2008)) used a sparse parameterization, with one or a few planes of uniform slip deficit defined and a coupling coefficient estimated to represent the slip deficit rate. Our own approach is closest to this end member approach, and we have adopted those results as long as they are not superseded by later studies. Other studies (e.g., Suito & Freymueller (2009)) estimated slip deficit on an array of small sub-faults, requiring substantial spatial smoothing in the inverse model. In these cases, we need to interpret the location of candidate section boundaries based on the spatial variations estimated in the model, define an average downdip width of the coupled patch and then average the slip deficit rate over our interpreted section. Additional studies use approaches that are intermediate between these two end members (e.g., Elliott & Freymueller, 2020; Drooff & Freymueller, 2021).

To generate geodetic recurrence values summarized in Table 2, we first generalize coupling values and map areas from previously published geodetic studies for each of the sections we define (Figure 2). In all cases, geodetic data is from onshore surveys. In some cases, such as for the Attu section, previously reported coupling values and the lateral extent of coupled polygons (Cross & Freymueller, 2008) nearly exactly match our representation. In other cases, we simplify and generalize the results of previous studies. For example, for the Prince William Sound section the results of Li et al., (2016) are represented here as a rectangular polygon with uniform coupling, while in reality the area is a complex mix of interseismic strain accumulation, slow slip events, and permanent deformation of the overriding plate, and the whole region is affected by 1964 postseismic movements. We based our estimate on the Li et al. (2016) model rather than the earlier Suito and Freymueller (2009) model because the more recent paper identified and modeled the changes in slip associated with the large multi-year slow slip events in Cook Inlet. The Elliott and Freymueller (2020) model shows similar boundaries for the Prince William Sound segment, but it uses several smaller fault segments to estimate a more spatially detailed slip deficit distribution. However, given that the 1964 earthquake appears to have ruptured the entire section as we have defined it, we opted to use the spatially simpler model and estimate the average slip deficit rate considering the estimates of all of the published studies.

We represent coupling polygons (Briggs, 2023) for each section with a buried, simplified, planar geometry for each section. This step is meant to convert from a plan-view representation of the coupled area to a three-dimensional polygon (dipping plane) for which we can calculate the area. These simple polygons are constructed to be consistent with geometries used in the ongoing USGS NSHM update for Alaska where the upper and lower depths are tied to the Slab2 model (Hayes et al., 2018). More complex approaches would use a curved interface, but we consider this simplification appropriate because the coupling patches are along the shallowest portion of the interface with generally little curvature, or restricted to narrow portions of the deeper interface. The plate interface or fault geometry is usually assumed rather than estimated in most studies of both interseismic slip deficit and coseismic slip, and where different studies do not use a model like Slab2, they often make different assumptions.

We next consider the appropriate plate convergence velocity to multiply by coupling to obtain the slip deficit rate. We start with relative Pacific-North America plate convergence velocities, and for sections west of Prince William Sound we correct these to relative Pacific-Bering velocities (Cross & Freymueller, 2008) centered along each fault section at the deformation front. This correction is small, and for most sections the Bering-North America motion is mostly trench-parallel. For sites in the Aleutians, there is an additional observed trench-parallel motion of the arc, which increases to the west (Cross & Freymueller, 2008). We removed the estimated trench-parallel arc velocity to derive the trench-perpendicular convergence (Pac-Arc OBS in Table 2). The Pac-Arc OBS values are identical to Pacific-Bering velocities (Figure 2) in the eastern portion of the AASZ (Yakataga to Sanak sections) but diminish to become only approximately half of the Pacific-Bering values in the far western portion of the AASZ, reflecting increasing obliquity of subduction in the west. Our assumption is that a substantial trench-parallel component of motion is accommodated by upper plate strike-slip faulting, such as the 2017  $M_w$  7.8 Komandorski Islands earthquake (Kogan et al., 2017;

Lay et al., 2017), but about half of the oblique relative plate motion is accommodated on the subduction interface based on Cross and Freymueller (2008).

The procedure described in the previous paragraph gives us the plate convergence rate that is most consistent with that actually modeled in most geodetic studies in the region (e.g., Cross & Freymueller, 2008). Some recent studies have made slightly different assumptions (or made slightly different estimates) about the motion of blocks on the overriding plate (e.g., Li & Freymueller, 2018; Elliott & Freymueller, 2020; Drooff & Freymueller, 2021), for example dividing the Bering Plate into a series of smaller blocks. However, most of the differences in block motions between the models are in the trench-parallel direction and no larger than a few mm/yr, which means they have only a very small effect on the estimated plate convergence rate. When comparing multiple studies for the same section, we compared estimated slip deficit rates rather than simply coupling coefficients, as the latter depends on the assumed plate convergence rate, but we express all results as coupling coefficients given the plate convergence rates in Table 2.

Once areas are calculated for each coupling polygon and trench-normal convergence is estimated for each fault section, we use scaling relations derived from Shaw (2023) to estimate a range of magnitudes, implied slip per magnitude, and recurrence values (Table 2). Our use of the Shaw (2023) model is intended to align with the NSHM update and also to illustrate the general approach of using scaling relations to estimate moment accumulation rates. The LogA scaling of Shaw (2023) reproduces the approach of (WGCEP, 2003) and is

$$M = \log_{10} A + C$$

where

$M$  is magnitude,  $A$  is area, and  $C$  is a constant for circular ruptures with constant stress drop.

Magnitudes  $M$  are obtained from area using three values of  $C$  recommended by (Shaw, 2023) for LogA scaling (4.1, 4.0, 3.9). In turn, the three magnitudes are converted to moment magnitudes  $M_0$  and implied slip per event ( $S$ ) from (Shaw, 2023) calculated as

$$S = M_0 / (A\mu) = 10^{1.5M + 9.05} / (A\mu)$$

where

$$\mu = \text{shear modulus} = 3 \cdot 10^{10} \text{ Pa}$$

Finally, recurrence is estimated by dividing implied slip per event by convergence rate multiplied by the coupling (Table 2).

In summary, we use plate convergence rates and a generalized depiction of geodetic coupling to characterize moment accumulation for each fault section and scaling relations to derive recurrence rates assuming area-magnitude scaling and implied slip per event. We do not propose that the coupled areas are exact proxies for rupture areas. Instead, our goal is to approximate the recurrence rates of reasonable ruptures per fault section generalized from the available geodetic data. In the 2023 update to the NSHM for Alaska, we anticipate that rupture areas will be relaxed and that the coupled polygons will not be the only ruptures considered in the model.

Below, we discuss each fault section from east to west. Because observations are relatively sparse in the context of the ~3,500-km-long subduction zone, section boundaries are not proposed as hard and persistent rupture boundaries, nor are the sections meant to imply only characteristic rupture behavior. In fact, the largest historical ruptures have typically involved two or more sections defined here, and lesser earthquakes have resulted from partial ruptures within or across fault sections (Fig. 2). It is expected that future approaches to modeling subduction zone seismic hazard in the AASZ will not rely on defining *ad hoc* rupture sections, but will vary ruptures to satisfy multiple constraints along strike (Field et al., 2020).

### 3 Results by fault section

#### 3.1 Yakataga section

The Yakataga section (Figure 3) extends ~ 150 km (measured along the deformation front) from Yakutat in the east to Cape Yakataga in the west. Although not a classic subduction interface, this section encompasses the easternmost end of AASZ subduction-related deformation where the Yakutat microplate is colliding obliquely with North America (Eberhart-Phillips et al., 2006) and models of geodetic strain allow for strain accumulation along the Yakutat plate interface (Elliott et al., 2013). Based on velocity models from crustal reflection and refraction studies, Worthington et al. (2012) interpret flat-slab subduction of the Yakutat terrane extending beyond the termination of the AASZ trench, from Kayak to Yakutat Bay. The  $M_w$  7.2 St. Elias earthquake may have ruptured a portion of a low-angle plate interface in this section (Estabrook et al., 1992). The western edge of this section is defined as the approximate location of a tear in subducting Yakutat crust interpreted from geophysical data and seismicity (Daly et al., 2021; Mann et al., 2022). The deformation front here is interpreted as coinciding with the Foreland Thrust system (Malaspina, Pamplona, and Esker Creek sections) (Worthington et al., 2008). The Wesson et al. (2007) model included a similar section (their Yakutat segment) to account for the possibility of a low-angle plate interface beneath the Yakataga fold-and-thrust belt.

It is unclear if coastal paleoseismic observations in the Yakataga section record slip on the Yakutat plate interface. Shennan et al. (2009, 2014) report paleogeodetic evidence for earthquakes at Yakutat Bay from the integration of marsh and landscape uplift at multiple sites spanning the inferred eastern edge of the 1964 rupture. Shennan et al. (2009) infer that the Yakataga section ruptured with the neighboring Prince William sound sections in ~870 BP and ~1440 BP, while also recognizing potential complications from upper plate faults such as the two  $> M_w$  8.0 Yakataga ruptures in September 1899. It is difficult to calculate a recurrence interval from only the ~870 BP and ~1440 BP events alone for which there is a single closed interval of 570 years, and so we estimate a [?]  $M_w$  8.5 open-interval recurrence of ~757  $\pm$  264 years.

Geodetic observations in the Yakataga section indicate a strong gradient in velocities between the coast and the Wrangell Mountains (Elliott & Freymueller, 2020; Elliott et al., 2013). Geodetic models place most of the strain in this area on upper-plate faults, except for a small patch of strain accumulation on the Yakutat decollement. In keeping with this interpretation, we depict a relatively small patch of coupled interface (~ 140 x 30 km polygon) far landward from the deformation front (30-75 km distance) that incorporates subsections of the Yakutat low-angle plate interface modeled by Elliott et al. (2013) and Elliott and Freymueller (2020), to which we assign 30% coupling (Figure 3, Table 2). Further work in this region would be beneficial to image coupling along the Yakutat plate interface and the interplay between upper plate and plate interface strain accumulation.

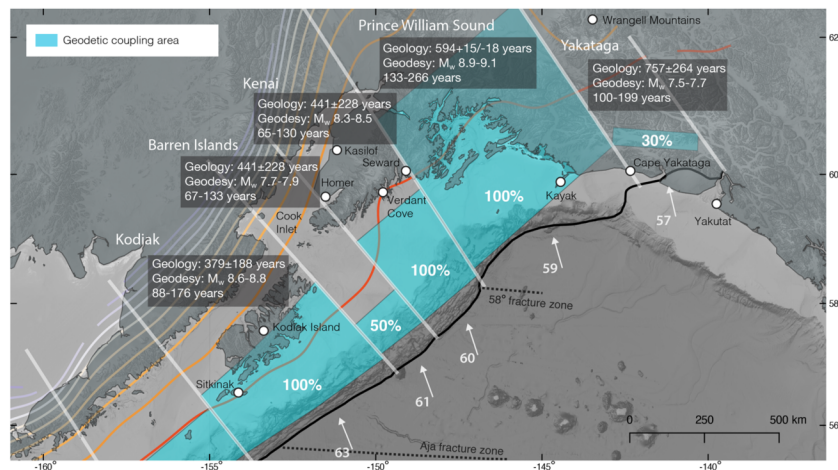


**Figure 3.** Detail of the Yakataga, Prince William Sound, Kenai, Barren Islands, and Kodiak sections along the AASZ. Geologic recurrence rates for  $M > 8.5$  rupture participation rates are from Table 1, and geodetic recurrence rates are from Table 2. Slab interface contours are from Hayes et al. (2018). Bathymetry and shaded relief from GEBCO Compilation Group (2023). Convergence vectors and coupling are as in Figure 2.

### 3.2 Prince William Sound section

The Prince William Sound section (Figure 3) extends  $\sim 320$  km between Bering Glacier and Seward and encompasses the region of maximum slip in 1964 (Ichinose et al., 2007; Suito & Freymueller, 2009). The plate interface is shallow here ( $\sim 6^\circ$ ) (Hayes et al., 2018; Worthington et al., 2012) reflecting subduction of the relatively buoyant Yakutat microplate with the Pacific Plate (Eberhart-Phillips et al., 2006) and leading to a wide seismogenic zone. Deep (60-80 km) nonvolcanic tremor located downdip from the 1964 rupture implies show, persistent slip along the interface between the Yakutat microplate and North America (Wech, 2016).

The geologic record of subduction earthquakes along the Prince William Sound section is well-established relative to the rest of the AASZ after many decades of paleoseismic studies (Carver & Plafker, 2008; Hamilton & Shennan, 2005a, 2005b; George Plafker et al., 1992). Marsh stratigraphy and geomorphologic studies show evidence for between seven (Shennan et al., 2014) and nine (Carver & Plafker, 2008) subduction ruptures along the Prince William Sound section since  $\sim 4$  to  $\sim 5$  ka. Recurrence intervals between the seven youngest ruptures range from  $\sim 420$  to 880 years, with the mean recurrence interval between the most recent six earthquakes of  $594 -15/+18$  years reported by Shennan et al. (2014) (Table 1).

Geodetic observations in the Prince William Sound section document a major slip patch in 1964 and a complex mix of subsequent postseismic and interseismic motions (Cohen & Freymueller, 1997; Li et al., 2016; Suito & Freymueller, 2009; Elliott & Freymueller, 2020). Strong coupling is attributed to shallow dip and geometric complexity at the easternmost end of the AASZ (Christensen & Beck, 1994). We simplify the available geodetic models and assume 100% interseismic coupling extending over 300 km inland from the trench, corresponding to a downdip limit of approximately 30 km depth (Li et al., 2016) (Figure 3). The depth and lateral extent of the segment are defined primarily from Li et al. (2016), which identified the presence of multi-year slow slip events in the Cook Inlet region. The Li et al. (2016) study distinguished between regions that have been persistently locked over the entire time span of geodetic observations, and regions of the interface that have accumulated slip deficit over certain time intervals and then released it in multi-year slow slip events. Other studies, such as Elliott & Freymueller (2020), used a single set of velocities and thus represent an average between the slow slip and non-slow slip intervals. The Elliott & Freymueller (2020) model estimated a more detailed upper plate block model than that assumed in Li et al. (2016), but this model also excluded some data from western Prince William Sound that was hard to fit. Some of the sites in southwest Prince William Sound move at nearly Pacific plate velocity, and all models persistently underestimate these observations unless the slip deficit rate is allowed to exceed the plate convergence rate. For example, Savage et al. (1998) used a plate convergence rate of 65 mm/yr, almost 20% too high, to model the observed velocities of a profile in western Prince William Sound (that study also did not account for postseismic deformation). In part due to the exclusion of some of the data from this profile, the Elliott & Freymueller (2020) model estimates a lower average slip deficit rate within parts of the Prince William Sound section than other studies did, but these variations all lie within the region of the massive Prince William Sound asperity as defined by coseismic slip models (e.g., Ichinose et al., 2007; Suito & Freymueller, 2009). Rather than subdivide the section further, we average the slip deficit over the whole polygon.

There is a discrepancy between the geodetic slip deficit rate and the observed geological recurrence rate for great earthquakes in Prince William Sound, as noted and discussed by Freymueller et al. (2008). The geologic recurrence interval (Table 1) is estimated to be  $594 \pm 20$  years (Carver & Plafker, 2008; Shennan et al., 2014), but given the observed plate convergence rate and 100% coupling coefficient required to fit the interseismic geodetic velocities, the geodetic estimate for  $M_w$  8.85 to 9.05 earthquakes is only  $\sim 200$ -

300 years, depending on assumptions. In short, a fully locked plate interface, which is clearly needed to fit the interseismic geodetic observations, would result in even more frequent great earthquakes than observed; Reducing the coupling coefficient to  $\sim 50\%$ , to match the geologic recurrence rate, would produce an enormous misfit to the geodetic data. The Elliott & Freymueller (2020) model includes significant permanent shortening of the upper plate, with the crustal block in Prince William Sound moving rapidly northward, and implying significant permanent contraction within the Chugach Mountains. However, that study excluded some of the data from SW Prince William Sound that were difficult to fit with any model (as noted above, those data were fit in earlier studies by allowing a slip deficit rate that exceeded the rate of plate motion). Some combination of permanent northward motion of the crustal block(s) in Prince William Sound (Elliott & Freymueller, 2020), a reduced incoming plate rate if the subducting crust is Yakutat Block rather than Pacific plate (Freymueller et al., 2008), or perhaps the occurrence of slow slip events to shallower depth than yet observed, or additional slip in  $M < \sim 8.5$  earthquakes that would be invisible in the geologic record would be required to explain the discrepancy. Future work would be necessary to fully explain the apparent mismatch between the geodetic and geologic record along the Prince William Sound section.

### 3.3 Kenai section

The Kenai section (Figure 3) extends approximately 125 km between Seward and Homer and lies between regions of major slip along the Prince William Sound and Kodiak sections in 1964. Pulpan & Frohlich (1985) suggested that the Kenai and adjacent Barren Islands sections (roughly their ‘Central Segment’) may exhibit different rupture behavior than the Prince William Sound and Kodiak sections due to tears in the downgoing slab. Hutchinson & Crowell (2007) examined regional archeological and paleoseismic ages and deduced that the Kenai section ruptures together with the adjacent PWS section but independently of the Kodiak section. Tape and Lomax (2022) show that the Kenai and neighboring Barren Islands section correspond to a local minimum in the spatial distribution of aftershocks of the 1964 rupture.

Paleoseismic data indicate that the Kenai section exhibits different rupture behavior than the neighboring Prince William Sound section. Mann & Crowell (1996) first documented a rupture at Verdant Cove  $\sim 800$  BP, and Kelsey et al. (2015) interpret this event as the 1060-1110 CE rupture identified by Shennan et al. (2014), which was initially interpreted as a multi-section rupture equal to or larger than the 1964 earthquake, but may have been a rupture centered only on Kodiak (Shennan et al., 2018). Kelsey et al. (2015) also identified evidence for an additional, younger earthquake at 1530-1840 CE. Several rupture scenarios fit the younger 1530-1840 CE data, including rupture with the adjacent Kodiak section, rupture in the historical 1788 event, or independent rupture of the Kenai section. Shennan et al. (2016) report peat-mud couplets at their Kasilof and Homer sites that may correspond to older subduction ruptures (e.g.,  $\sim 2050$  BP), although more study would be useful to develop the earthquake chronology at these sites. We limit our analysis to the chronology of Kelsey et al. (2015), which provides a closed-interval mean recurrence of  $\sim 441$  years (Table 1).

Geodetic observations along the Kenai section show that the interface is highly coupled but that the width of coupling is much less than the neighboring Prince William Sound section and confined to mostly near the trench (Freymueller et al., 2000; Li et al., 2016; Suito & Freymueller, 2009). Here we model a 100% coupled seismogenic zone extending  $\sim 225$  km from the trench with a downdip depth of  $\sim 20$  km (Li et al., 2016) (Figure 3).

### 3.4 Barren Islands section

The Barren Islands section (Figure 3) is the narrowest section we define along strike ( $\sim 95$  km), and this stretch of the subduction interface appears to have slipped very little in 1964 (Ichinose et al., 2007; Suito & Freymueller, 2009) and is poorly coupled from geodetic observations (Freymueller et al., 2000); (Suito & Freymueller, 2009) (Li et al., 2016). Ye et al. (1997) interpret a 20-km-thick underplated low-velocity zone along the Barren Islands section, and von Huene et al. (1999) infer that the  $58^\circ$  fracture zone may modulate rupture here and in the adjoining Kenai section.

No paleoseismic data from the Barren Islands section are available. We infer that this section ruptures with neighboring sections, as in 1964, and that geologic recurrence is similar to the neighboring Kenai section

(closed-interval mean recurrence of  $\sim 441$  years) (Table 1). Geodetic data are interpreted as consistent with a relatively small ( $\sim 95 \times \sim 75$  km) near-trench patch with 50% coupling (Figure 3), and this section is differentiated in our model because of this coupling difference and the relative lack of slip in 1964.

### 3.5 Kodiak section

The Kodiak section (Figure 3) extends  $\sim 310$  km along Kodiak Island to just beyond the Trinity Islands and encompasses a major slip patch in the CE 1964 rupture (Ichinose et al., 2007; Suito & Freymueller, 2009). The Kodiak section also exhibits a larger area of high interseismic coupling than the adjacent Barren Islands and Kenai sections (Li et al., 2016). The slab dip beneath Kodiak is steeper, and the seismogenic interface correspondingly narrower, than the neighboring Barren Islands, Kenai, and Prince William Sound sections (Hayes et al., 2018). Slip in 1964 terminated near Sitkinak Island southwest of Kodiak (Briggs et al., 2014; Plafker, 1969), corresponding roughly with the intersection of the Aja fracture zone and the accretionary prism (von Huene et al., 1999).

The Kodiak section has been the focus of many detailed paleoseismic investigations (Carver & Plafker, 2008; Gilpin, 1995; Gilpin et al., 1994; Shennan et al., 2014). Shennan et al. (2018) summarize evidence for five Kodiak-section-wide land-level changes between 1964 CE and  $\sim 1500$  BP, including the historical penultimate event in 1788, resulting in a mean closed-interval recurrence of  $\sim 379$  years (Table 1). Observations from sites spanning the 1964 rupture zone indicate that the Kodiak section typically ruptures independently of the Prince William Sound section (Shennan et al., 2018).

Geodetic observations along the Kodiak section are consistent with a highly coupled interface beneath Kodiak Island (Drooff & Freymueller, 2021; Li et al., 2016; Li & Freymueller, 2018). Here we generalize the geodetic models into 100% coupling extending  $\sim 175$  from the deformation front, corresponding to a locking depth of  $\sim 30$  km on the plate interface (Figure 3).

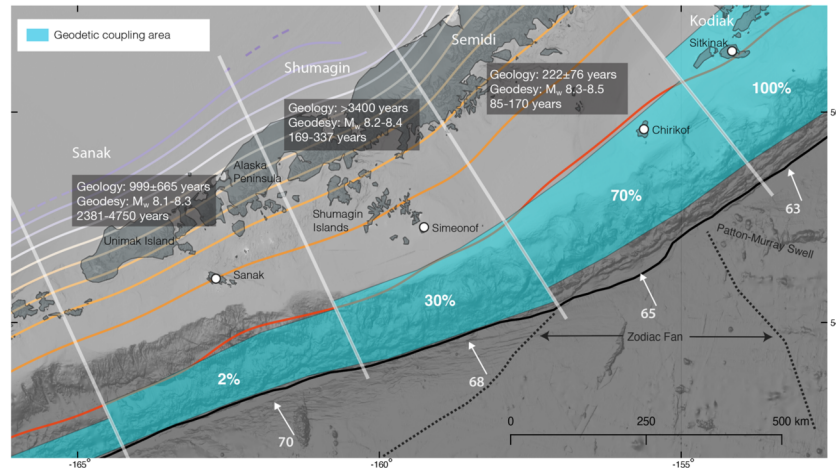


**Figure 4.** Detail of the Semidi, Shumagin, and Sanak sections along the AASZ. Geologic recurrence rates for  $M > 8.5$  rupture participation rates are from Table 1 and geodetic recurrence rates are from Table 2. Slab interface contours are from Hayes et al (2018). Bathymetry and shaded relief from GEBCO Compilation Group (2023). Convergence vectors and coupling are as in Figure 2.

### 3.6 Semidi section

The Semidi section (Figure 4) extends  $\sim 250$  km from approximately the southwestern edge of the 1964 CE rupture near Sitkinak Island to  $\sim 70$  km east of the Shumagin Islands (Nishenko & Jacob, 1990). The Semidi section is differentiated from the neighboring Kodiak and Shumagin sections based on historical and paleoseismic earthquake history: this portion of the AASZ hosted great historical ruptures in 1938 ( $M_w$  8.3) and 2021 ( $M_w$  8.2) (Elliott et al., 2022; Freymueller et al., 2021), although these appear to be much smaller than the 1788 rupture from paleoseismic records (Briggs et al., 2014; Nelson et al., 2015). We draw the boundary between the Semidi and the adjacent Shumagin segment based on the presumed western edge of the 2021  $M_w$  8.2 Chignik earthquake (Elliott et al., 2022), which also corresponded to a segment boundary in the interseismic model of Drooff and Freymueller (2021). von Huene et al. (1999) infer that the Patton-Murray hot spot swell may influence rupture character of the Semidi section, which exhibits much higher interseismic coupling than the Shumagin section to the southwest; alternatively, von Huene et al. (2012) also argue that the subduction of the head of the Zodiac fan may influence rupture behavior in this section. The Semidi section was recognized as a potential source for a Pacific basin-wide tsunami with risk implications for the western coast of the United States (Ross et al., 2013).

The geologic record of subduction earthquakes for the Semidi section is derived from geologic studies on Chirikof and Sitkinak Islands. On Chirikof Island, stratigraphic evidence of 13 paleotsunamis since  $\sim 3.5$  ka, including the major historical 1788 rupture, corresponds to a paleotsunami recurrence of 180-270 years (Nelson et al., 2015). Sitkinak is at the westernmost edge of the neighboring Kodiak section, and so is not strictly in the Semidi section; however, marshes at Sitkinak record a series of land level changes that we infer record ruptures of the Semidi section. Five land-level changes at Sitkinak (Briggs et al., 2014), between  $\sim 1050$  BP and 1788 CE indicate a recurrence interval of  $\sim 222$  years, in agreement with the paleotsunami record from Chirikof (Table 1).

Geodetic observations in the Semidi section consistently show a highly coupled region with a lower coupling toward the Shumagin islands to the west (Drooff & Freymueller, 2021; Li & Freymueller, 2018). Li & Freymueller (2018) estimated strong coupling in their ‘Semidi segment’ ( $\sim 70\%$ ), with much lower coupling to the west in their ‘Shumagin segment’ ( $\sim 40\%$ ). However, few data were used to constrain the location of the boundary, so the location was quite uncertain. Drooff and Freymueller (2021) revised the segment boundaries of Li and Freymueller (2018), incorporating additional data from Veniaminof volcano on the Alaska Peninsula, which had been excluded in the earlier study due to the presence of volcanic deformation. Drooff and Freymueller (2021) shifted the western boundary of the Semidi section to the east, leaving strong coupling in their segment 2, and broke the Shumagin region into two segments (their segments 3 and 4). Our location of the Semidi-Shumagin boundary corresponds to the boundary between the Drooff and Freymueller (2021) segments 2 and 3, which also corresponds closely to the southwestern edge of the 2021 rupture. For hazard estimates, we represent 70% coupling  $\sim 125$  km from the deformation front, corresponding to a locking depth on the Slab2 interface of  $\sim 20$  km (Figure 4). The slip deficit at shallow depth near the trench is highly uncertain due to poor model resolution, and depends strongly on the assumed model regularization (Xiao et al., 2021), but the total integrated moment accumulation rate does not vary much even where the appearance of the slip deficit distribution with depth varies a lot. Because we lack concrete information about whether the shallow part of the interface is locked or creeping, we adopt the estimates based on models that assume locking to the trench.

### 3.7 Shumagin section

The  $\sim 220$  km Shumagin section (Figure 4) encompasses the Shumagin Islands and was long presumed to be a seismic gap with high potential for hosting future large earthquakes (Davies et al., 1981; McCann et al., 1979; Nishenko & Jacob, 1990). However, subsequent geodetic data in the Shumagin Islands are consistent with a poorly coupled plate interface (Freymueller & Beavan, 1999; Lisowski et al., 1988; Savage et al., 1986) and geologic observations at Simeonof Island do not find evidence for substantial land-level changes or tsunami runup since  $\sim 3.4$  ka (Witter et al., 2014). Historical ruptures have been relatively small in the context of the largest AASZ earthquakes, including the 1948  $M_w$  7.5 and 2020  $M_w$  7.8 events (Estabrook & Boyd, 1992; Ye et al., 2022) (Figure 1).

Li & Freymueller (2018) examined lateral variations of locking in this region, and we generalize their findings as 30% coupling extending  $\sim 80$  km from the deformation front, corresponding to a locking depth on the interface of  $\sim 20$  km (Figure 4). Drooff and Freymueller (2021) divided the region of this section into two distinct segments, one with  $\sim 40\%$  coupling and one with  $\sim 20\%$ . The 2020  $M_w$  7.8 Shumagin Islands earthquake broke across both of those segments, with higher average slip in the eastern part (Xiao et al., 2021); the boundary between the higher and lower slip parts of the rupture corresponds to the interseismic boundary as defined by Drooff and Freymueller (2021). Our Shumagin section corresponds roughly to the extent of the 2020  $M_w$  7.8 Shumagin Islands earthquake, so we chose not to subdivide the section further. Averaged over the whole section, the models of Li & Freymueller (2018) and Drooff & Freymueller (2021) give the same results. Because we lack concrete information about whether the shallow part of the interface is locked or creeping, we adopt the estimates based on models that assume locking to the trench (Xiao et al., 2021).

### 3.8 Sanak section

The Sanak section (Figure 4) extends  $\sim 275$  km and hosted the 1946  $M_w$  8.6 Unimak Island earthquake, which spawned a devastating local and trans-Pacific tsunami (Okal & Hébert, 2007). Shallow slip on the megathrust extending to near the deformation front in 1946 is inferred based on teleseismic, tsunami, and aftershock observations (Johnson & Satake, 1997; Okal & Hébert, 2007; Tape & Lomax, 2022). We follow Fournier and Freymueller (2007) in recognizing the Sanak section as distinct from the neighboring Shumagin section based on historical rupture and geodetic observations.

The geologic record of earthquakes is limited to reconnaissance studies on Sanak Island (Engelhart et al., 2015), which had stratigraphic evidence for the 1946 tsunami, a hiatus from 1946 to  $\sim 2$ ka, and then 4 tsunami sand sheets from  $\sim 4$ ka to  $\sim 2$ ka. This implies a mean tsunami recurrence of  $\sim 1,000 \pm 665$  years spanning  $\sim 4$ ka to 1946 (assuming equal intervals between 4 ka and 2 ka) (Table 1), presuming that the older sand sheets are due to a proximal source and therefore analogous to the sand sheet associated with the 1946 rupture.

Geodetic observations in the Sanak section (Fournier & Freymueller, 2007; Freymueller & Beavan, 1999; Li & Freymueller, 2018) imply a nearly freely slipping plate interface. We assign 2% coupling extending  $\sim 50$  km from the deformation front, with a locked depth on the interface of  $\sim 20$  km (Figure 4). In the western part of the Sanak segment, geodetic data are restricted to the Alaska Peninsula and Unimak Island, as no islands are offshore in the forearc, and thus geodetic model resolution for the offshore region is very poor. It is likely that the high slip region of the 1946 earthquake (Lopez & Okal, 2006) occurred mainly in the western part of this section, where geodetic constraints on near-trench slip deficit are minimal. However, to date no source model for the 1946 earthquake has been presented that is also consistent with the lack of observed geodetic strain.

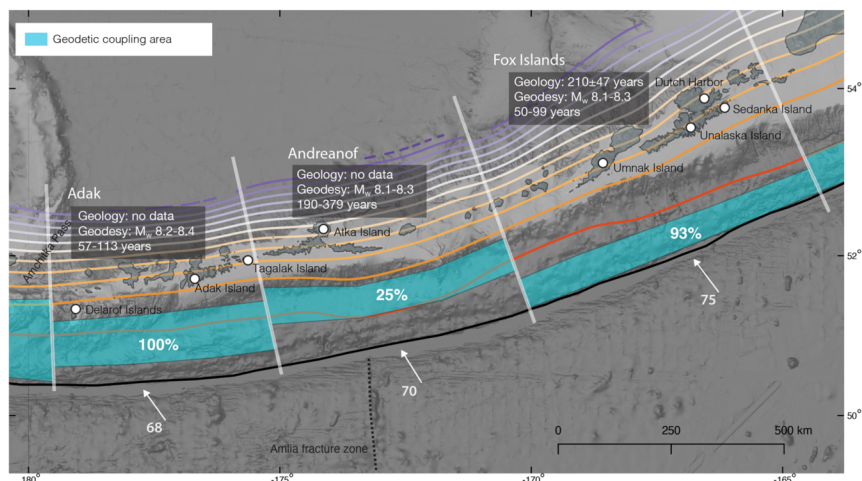


**Figure 5.** Detail of the Fox Islands, Andreanof, and Adak sections along the AASZ. Geologic recurrence rates for  $M > 8.5$  rupture participation rates are from Table 1, and geodetic recurrence rates are from Table 2. Slab interface contours are from Hayes et al. (2018). Bathymetry and shaded relief from GEBCO Compilation Group (2023). Convergence vectors and coupling are as in Figure 2.

### 3.9 Fox Islands section

The 1957  $M_w$  8.6 rupture spanned  $\sim 1,230$  km and three of the sections defined here (Fox Islands, Andreanof, and Adak) (Johnson & Satake, 1993; Tape & Lomax, 2022). The  $\sim 425$  km Fox Islands section (Figure 5) was the location of the easternmost extent of slip in 1957 modeled by Johnson & Satake (1993), although the amount and location of slip based on the teleseismic data is uncertain, and the depiction of the easternmost portion of the 1957 rupture varies substantially among studies (McCann et al., 1979; Tape & Lomax, 2022). Tsunami models of Nicolovsky et al. (2016) show that shallow (5–15 km) rupture in the Fox Islands section in 1957 most closely reproduces the 1957 Dutch Harbor tide gage observations and nearby  $>18$  m runup at Sedanka Island.

The geologic record of interface ruptures is inferred from paleotsunami data at sites on Umnak and Sedanka Islands (Witter et al., 2016, 2019). The two sites record four previous tsunamis similar to the 1957 event, implying a 164- to 257-year recurrence interval of tsunamigenic ruptures (Table 1) (Witter et al., 2019). The five tsunamis interpreted as coeval at the Umnak and Sedanka Islands are remarkable for their water height (up to 15–23 m above modern sea level) and inundation, and are interpreted as representing subduction interface ruptures similar in magnitude to 1957 of  $M_w$  8.6 or larger. An important finding of the geologic studies on the Fox Islands is that similar to 1957, past ruptures appear to have crossed an apparent transition between regions with variable coupling (Witter et al., 2019). This indicates that our assumption that coupling is constant for hazard purposes may be an oversimplification. However, no geodetic data constrain time-varying coupling in the region.

Similar to other locations with observations far from the deformation front, geodetic data in the Fox Islands section can be fit by multiple models, including those that place complete or nearly complete locking over a narrow patch close to the trench (Xue & Freymueller, 2020) or lower values of coupling on a deeper patch (Cross & Freymueller, 2008). Because Nicolovsky et al. (2016) found the best model fit to the 1957 tsunami required predominantly shallow slip on the interface, we draw primarily from Xue and Freymueller (2020) and model 93% coupling extending  $\sim 40$  km arcward from the deformation front, corresponding to a depth of  $\sim 15$  km along the subduction interface (Figure 5).

### 3.10 Andreanof section

The Andreanof section (Figure 5) extends ~350 km and is centered along the 1,230 km-long aftershock zone of the 1957 rupture (Tape & Lomax, 2022), a region of apparently little to no coseismic slip in 1957 (Johnson & Satake, 1993). The Amlia fracture zone intersects roughly the center of this section and has been hypothesized to have a major influence on upper plate structure and interface coupling (Ryan et al., 2012). Whether the Amlia fracture zone modulated slip in the 1957 earthquake is unclear, but it did not arrest rupture (Sykes, 1971). The Amlia fracture zone roughly corresponds to the eastern edge of the aftershock extent of the 1986  $M_w$  7.9 Andreanof Islands earthquake (Figure 2), which ruptured mainly the neighboring Adak section (Tape & Lomax, 2022).

At present, no paleoseismic records are available from the Andreanof Islands westward along the Alaska-Aleutian subduction zone, and so recurrence values are estimated from geodetic data alone for these sections. Geodetic observations in the western Aleutians came primarily from a geodetic campaign network started in the 1990s by Ave Lallemand & Oldow (2000) and by the USGS Alaska Volcano Observatory, with results summarized by Freymueller et al. (2008).

Geodetic data from the Andreanof section show that this section is, on average, poorly coupled based on sparse observations (Cross & Freymueller, 2008). We generalize the results of Cross and Freymueller (2008) by modeling 25% coupling along a polygon spanning approximately 20-35 km depth on the interface (Figure 5).

### 3.11 Adak section

The Adak section extends ~315 km from Tagalak Island to Amchitka Pass (Figure 5) and is the westernmost portion of the 1957 rupture and the location of the highest values of coseismic slip (Johnson & Satake, 1993). The Adak section also encompasses the main slip areas of two notable  $M_w$  7.9 aftershocks of the 1957 rupture in 1986 and 1996 (Boyd & Nábělek, 1988; Tanioka & Gonzalez, 1998; Tape & Lomax, 2022) (Figure 1).

From the Adak section westward, a substantial component of arc-parallel motion is observed in interseismic velocities at island Global Navigation Satellite Systems (GNSS) sites (Cross & Freymueller, 2008). These motions reflect oblique convergence between the Pacific and North America plates and the transition of the subduction margin to a composite transform-convergent plate boundary (Ryan & Coleman, 1992) resulting in translations of arc slivers along strike-slip faults and block rotations in the overriding plate (Geist et al., 1988; Avé Lallemand, 1996).

Because plate convergence become increasingly oblique in the west AASZ, we report plate convergence rates (Table 2) that reflect observed Pacific-Arc trench-perpendicular rates, which account for translation of arc slivers relative to the Bering plate (Cross & Freymueller, 2008).

Geodetic observations in the Adak section from Adak Island can be modeled with 100% coupling of a small portion of the interface, while those from the Delarof Islands indicate less updip coupling in the western part of the section (Cross & Freymueller, 2008). Because of the historical seismicity in the region, we give priority to the Adak Island observations and infer 100% coupling extending to ~30 km on the plate interface (Figure 5).

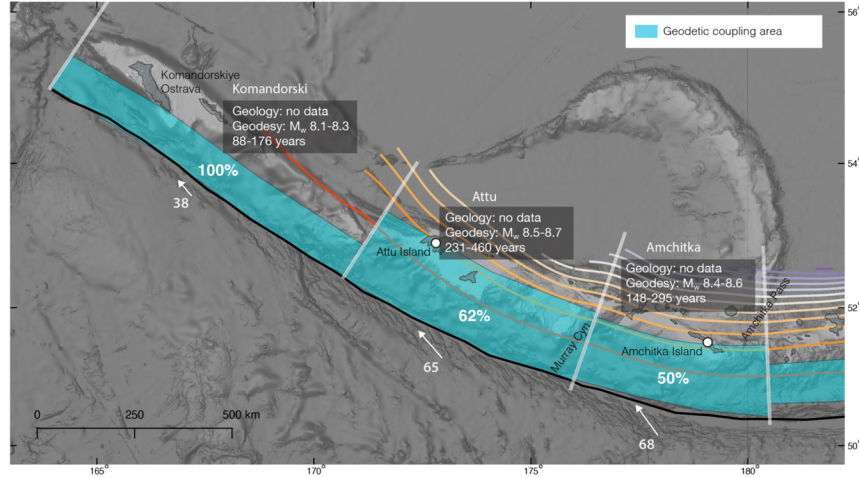


**Figure 6.** Detail of the Amchitka, Attu, and Komandorski sections along the AASZ. Geologic recurrence rates for  $M > 8.5$  rupture participation rates are from Table 1 and geodetic recurrence rates are from Table 2. Slab interface contours are from Hayes et al. (2018). Bathymetry and shaded relief from GEBCO Compilation Group (2023). Convergence vectors and coupling are as in Figure 2.

### 3.12 Amchitka section

The Amchitka section (Figure 6) extends  $\sim 325$  km from Amchitka Pass to Murray Canyon and encompasses the eastern portion of the  $M_w$  8.7 1965 Rat Islands rupture, as well as the area of the much smaller 2003  $M_w$  7.8 earthquake (Figure 1). The Amchitka section corresponds to the hypothesized Rat structural block of (Geist et al., 1988) and one of three asperities in the 1965 event proposed by Beck & Christensen (1991).

Geodetic observations in the Amchitka section are sparse (Cross & Freymueller, 2008) and no direct coupling model is available. Based on the neighboring Attu section, we infer 50% coupling over an area roughly the same as the Attu section, extending  $\sim 115$  km arcward from the deformation front to approximately 40 km interface depth (Figure 6).

### 3.13 Attu section

The Attu section (Figure 6) extends  $\sim 400$  km from Murray Canyon to the western terminus of the 1965  $M_w$  8.7 rupture. It encompasses the hypothesized Buldir and Near blocks of Geist et al. (1988) and two of the three high-slip asperities in the 1965 event proposed by Beck and Christensen (1991).

We directly incorporate the model of Cross & Freymueller (2008) depicting 62% coupling extending  $\sim 120$  km arcward from the deformation front, corresponding to a lower depth of  $\sim 40$  km along the subduction interface (Figure 6).

### 3.14 Komandorski section

The Komandorski section (Figure 6) extends  $\sim 530$  km from near the western edge of Attu to the western end of the AASZ. Although this section is not included in the USGS NSHM, we include it here for completeness. There is no historical subduction interface rupture larger than  $M_w$  6 or deeper than 50 km recorded along this section of the subduction zone (Kogan et al., 2017), nor is there active volcanism (Newberry et al., 1986). The 2017  $M_w$  7.8 earthquake near Komandorskiy Ostrova (also known as Komandorski Islands) in

Russia ruptured nearly 400 km of the strike-slip Bering fracture zone between the Komandorski sliver and the Bering plate (Lay et al., 2017).

A substantial component of relative Pacific-Bering plate convergence is arc-parallel in the Komandorski section. Modeled geodetic observations indicate that lateral motion is accommodated along primarily along backarc strike-slip faulting as demonstrated in the 2017  $M_w$  7.8 rupture, but also as oblique convergence along the shallow subduction interface (Kogan et al., 2017; Lay et al., 2017). It is unclear if shallow interface slip is completely strike-slip as depicted in Lay et al. (2017), or if it is oblique or even occasionally trench-normal on the interface. Given the occurrence of subduction interface slip near the Andaman Islands (India) in the  $M_w$  9.15 Sumatra–Andaman earthquake of 2004 where the Indian Plate converges obliquely under the Andaman Islands (Chlieh et al., 2007), we do not discard the idea that highly oblique relative plate convergence can lead to interface slip.

Geodetic observations in the Komandorski section can be fit with a model of a rigid Komandorski sliver moving westward at  $\sim 51$  mm/year, bounded by the Aleutian subduction interface to the south and by the Bering fracture zone to the north (Kogan et al., 2017). Our calculation of relative Pacific - arc velocities (Table 2) indicates that as much as 38 mm/yr of convergence is available for interface slip. In the context of these models, we infer 100% coupling on the shallow subduction interface from the deformation front to a map distance of  $\sim 55$  km arcward, corresponding to a depth of  $\sim 15$  km (Figure 6).

### 3.15 Summary of geologic and geodetic recurrence estimates

We present a summary of the geologic and geodetic recurrence estimates discussed in this section in Tables 1 and 2. Table 1 reflects the recurrence of presumably  $> M_w$  8.5 ruptures for each fault section, and illustrates that paleogeologic and paleotsunami data are available for only the eastern AASZ. Table 2 contains geodetic recurrence estimates from the convergence rates, coupling values, and coupled areas for each section, using the scaling relations of Shaw (2023).

## 4 Discussion

The recurrence estimates reported here range from  $\sim 220$  years (Semidi section) to  $\sim 1000$  years (Sanak section) for  $M_w$  [?] 8.5 events from geologic data (Table 1) and from 50 years ( $M_w$  8.1, Fox Islands section) to 4750 years ( $M_w$  8.3, Sanak section) from geodetic data (Table 2). The two approaches provide different, but complementary, views of rupture behavior. Along the energetic coasts of Alaska, geologic data capture only the largest ruptures, generally with preserved evidence of vertical deformation above detection limits of  $>0.2$  m (Hawkes et al., 2010; Shennan et al., 2016) or tsunami runup  $> 5$  m above the modern tidal range (Nelson et al., 2015; Witter et al., 2016, 2019). The geologic data also represents events that typically rupture multiple fault sections, which is demonstrated by historical events and inferred for prehistoric earthquakes – in this regard, the geologic recurrence rates should be viewed as participation rates in ruptures  $>M_w$  8.5 for each fault section for which geologic data are available. The geodetic data are used to approximate strain accumulation and release by single fault section, and so recurrence rates of these events are necessarily shorter and the inferred earthquake magnitudes are smaller than events recorded by geology.

A primary advantage of the geodetic recurrence model is that it estimates moment accumulation on the model subduction interface sections in a general way. Because coupling magnitude and coupled area generally trade off in geodetic models, the exact location of the coupled patches is not critical. Instead, our goal is to estimate the moment accumulation budget available for interface ruptures, rather than using geodesy to strictly define rupture patches. By calculating the recurrence on sections we have defined *a priori*, we provide information that can be interpreted in the broader context of section magnitude frequency distributions and multi-section ruptures. The coupling polygons we present here are not meant to strictly correlate with rupture patches. Complex non-unique coupling models are often presented for subduction zone interfaces, including for some portions of the AASZ (Li et al., 2016), and the relation between interseismic coupling and interface

ruptures can be modeled in intricate ways (Small & Melgar, 2021). However, the relation between geodetic coupling models (strain accumulation) and eventual rupture (strain release) is not straightforward, and the assumption that complex depictions of interseismic coupling uniquely predict future rupture patterns is not clearly supported (Noda and Lapusta, 2013; Tsang et al., 2015; Witter et al., 2019). For example, persistent asperity models such as most recently presented by Zhao et al. (2022) for the Shumagin and Semidi sections of the AASZ use recent ruptures to create non-unique backslip scenarios that fit sparse GNSS measurements reasonably well. These models offer limited utility for hazard forecasts because they effectively predict characteristic earthquakes (Schwartz, 1999) unless the persistent asperity assumption is relaxed and modified (Avouac, 2015), and a primary objective in modern seismic hazard modeling is to move beyond the assumption that past earthquakes uniquely predict future ruptures (Field et al., 2014).

Our effort to assign recurrence values along the AASZ points to several potential future studies and opportunities. Geologic studies would be beneficial to characterize rupture behavior in the western ~1,250 km of the subduction zone, for which no data are currently available. Geodetic data are fundamentally important for understanding subduction zone hazard, and a denser permanent GNSS network throughout the AASZ would improve hazard estimates – and especially on the seafloor, where recent GNSS-Acoustic studies (Brooks et al., 2023) have demonstrated the importance of seafloor geodesy. Instead of a single model, future coupling and slip-deficit models from geodesy might be presented as a suite of models that encompass the broadest possible range of uncertainty, such as multiple geodetic models presented in Schmalzle et al. (2014) and Marinier et al. (2021).

The AASZ experienced a series of major ruptures in the 20th century along much of its length. Recurrence intervals for these largest ruptures are many centuries long, and it was previously assumed that apparently unruptured portions of the interface in the historical period, or seismic gaps (Davies et al., 1981), would be most likely to host future ruptures, and conversely, that regions that ruptured in the 20th century were likely no longer hazardous in the 21st century. However, re-rupture of a historical great earthquake rupture patch by subsequent large events has been documented or inferred along the AASZ (Schwartz, 1999; Tanioka & Gonzalez, 1998; Brooks et al., 2023). Complex rupture overlap is also supported by current observations and models of subduction interface frictional behavior, which demonstrate that subduction interfaces are a mosaic of slip patches along strike and down dip (Lay et al., 2012). The regions of interface slip associated with historical events are very poorly known (Nicolisky et al., 2016; Witter et al., 2019) and the extremely generalized historical rupture areas from aftershocks (Tape & Lomax, 2022) and coarse rupture models (Johnson & Satake, 1993) are insufficient to accurately define historical slip patches. Our recurrence results indicate that most sections we define along the AASZ are capable of  $> M_w$  8 ruptures roughly every century, and that the locations of historical ruptures and presumed spatial variations in interseismic coupling are only loose constraints on future rupture locations and magnitudes.

## 5 Summary

We present recurrence estimates from geologic and geodetic data for the Alaska-Aleutian subduction zone, summarized by fault section. Fourteen fault sections divide the subduction interface into 95- to 540-km-long portions that reflect observed or inferred trends in rupture behavior along strike, geodetic coupling, and geologic structure. The recurrence estimates can be used to provide constraints for seismic hazard models. Geologic data are interpreted as reflecting the relatively rarer (~220 - 1,000 year) participation of model fault sections in  $M_w$  [?] 8.5 ruptures, while geodetic data are consistent with moment accumulation rates corresponding to much more frequent (~50 - 250 year) recurrence of  $M_w$  8.0 - 8.5 ruptures along most fault sections. Our analysis indicates that the rates of  $M_w$  [?] 8 ruptures is higher than previously assumed, especially west of Kodiak Island where geologic and geodetic data have not previously been considered together.

## Data Availability Statement

The coupling polygons can be accessed at <https://doi.org/10.5066/P9H2PE6W> (Briggs, 2023).

## Acknowledgements

We gratefully acknowledge the ideas and discussion from participants during the U.S. Geological Survey John Wesley Powell Center for Analysis and Synthesis working group on Tsunami Source Standardization for Hazards Mitigation in the United States meeting in 2018 on Alaska Aleutian subduction zone tsunami sources, in coordination with the National Tsunami Hazards Mitigation Program (NTHMP), led by Stephanie L. Ross (USGS Pacific Coastal and Marine Science Center) and core group members Marie Eble (National Oceanic and Atmospheric Administration), Pat Lynett (University of Southern California), Dmitry J. Nicolsky (University of Alaska Fairbanks), Kenny Ryan (Air Force Research Laboratory), Hong Kie Thio (AECOM), and Rick Wilson (California Geological Survey). We thank Julie Elliott (Michigan State University) for discussions regarding geodetic data and models. We thank Harvey Kelsey, Alex Hatem, two anonymous reviewers, and Associate Editor Natalia Ruppert for their helpful suggestions. Any use of trade, firm, or product names is for descriptive purposes only and does not imply endorsement by the U.S. Government.

## References

- Adams, J. (1990). Paleoseismicity of the Cascadia subduction zone: Evidence from turbidites off the Oregon-Washington margin. *Tectonics*, *9* (4), 569-583. <https://doi.org/10.1029/TC009i004p00569>
- Atwater, B. F. (1987). Evidence for great Holocene earthquakes along the outer coast of Washington State. *Science*, *236* (4804), 942-944. <https://doi.org/10.1126/science.236.4804.942>
- Avé Lallemant, H. G. (1996). Displacement partitioning and arc-parallel extension in the Aleutian volcanic island arc. *Tectonophysics*, *256* (1), 279-293. [https://doi.org/10.1016/0040-1951\(95\)00171-9](https://doi.org/10.1016/0040-1951(95)00171-9)
- Avé Lallemant, H. G., & Oldow, J. S. (2000). Active displacement partitioning and arc-parallel extension of the Aleutian volcanic arc based on Global Positioning System geodesy and kinematic analysis. *Geology*, *28* (8), 739-742. [https://doi.org/10.1130/0091-7613\(2000\)28<739:ADPAAE>2.0.CO;2](https://doi.org/10.1130/0091-7613(2000)28<739:ADPAAE>2.0.CO;2)
- Avouac, J.-P. (2015). From geodetic imaging of seismic and aseismic fault slip to dynamic modeling of the seismic cycle. *Annual Review of Earth and Planetary Sciences*, *43* (1), 233-271. <https://doi.org/10.1146/annurev-earth-060614-105302>
- Barnhart, W. D., Murray, J. R., Briggs, R. W., Gomez, F., Miles, C. P. J., Svarc, J., et al. (2016). Coseismic slip and early afterslip of the 2015 Illapel, Chile, earthquake: Implications for frictional heterogeneity and coastal uplift. *Journal of Geophysical Research: Solid Earth*, *121* (8), 6172-6191. <https://doi.org/10.1002/2016JB013124>
- Beck, S. L., & Christensen, D. H. (1991). Rupture process of the February 4, 1965, Rat Islands Earthquake. *Journal of Geophysical Research: Solid Earth*, *96* (B2), 2205-2221. <https://doi.org/10.1029/90JB02092>
- Boyd, T. M., & Nábělek, J. L. (1988). Rupture process of the Andreanof Islands earthquake of May 7, 1986. *Bulletin of the Seismological Society of America*, *78* (5), 1653-1673. <https://doi.org/10.1785/BSSA0780051653>
- Briggs, R. W., Engelhart, S. E., Nelson, A. R., Dura, T., Kemp, A. C., Haeussler, P. J., et al. (2014). Uplift and subsidence reveal a non-persistent megathrust rupture boundary (Sitkinak Island, Alaska). *Geophysical Research Letters*, *41* (7), 2289-2296. <https://doi.org/10.1002/2014GL059380>
- Briggs, R.W., (2023), Geodetic polygons for an Alaska-Aleutian subduction zone interface earthquake recurrence model. *U.S. Geological Survey data release* . <https://doi.org/10.5066/P9H2PE6W>
- Brooks, B.A., Goldberg, D., DeSanto, J., Ericksen, T.L., Webb, S.C., Nooner, S.L., et al. (2023). Rapid shallow megathrust afterslip from the 2021 M8.2 Chignik, Alaska earthquake revealed by seafloor geodesy. *Science*

*Advances*, 9 (17), eadf9299. <https://doi.org/10.1126/sciadv.adf9299>

Carver, G., & Plafker, G. (2008). Paleoseismicity and neotectonics of the Aleutian subduction zone—An overview. In: J. T. Freymueller, P. J. Haeussler, R. L. Wesson, & G. Ekström (Eds.) *Active Tectonics and Seismic Potential of Alaska: Geophysical Monograph Series 179* (pp. 43-63), Washington, D.C.: American Geophysical Union. <https://doi.org/10.1029/179GM03>

Chlieh, M., Avouac, J. P., Hjorleifsdottir, V., Song, T. R. A., Ji, C., Sieh, K., et al. (2007). Coseismic slip and afterslip of the great Mw 9.15 Sumatra–Andaman earthquake of 2004. *Bulletin of the Seismological Society of America*, 97 (1A), S152-S173. <https://doi.org/10.1785/0120050631>

Chlieh, M., Avouac, J. P., Sieh, K., Natawidjaja, D. H., & Galetzka, J. (2008). Heterogeneous coupling of the Sumatran megathrust constrained by geodetic and paleogeodetic measurements. *Journal of Geophysical Research: Solid Earth*, 113 (B5), B05305. <https://doi.org/10.1029/2007JB004981>

Christensen, D. H., & Beck, S. L. (1994). The rupture process and tectonic implications of the great 1964 Prince William Sound earthquake. *Pure and Applied Geophysics*, 142 (1), 29-53. <https://doi.org/10.1007/BF00875967>

Coffey, G. L., Rollins, C., Van Dissen, R. J., Rhoades, D. A., Thingbaijam, K. K. S., Clark, K. J., et al. (2022). *New Zealand National Seismic Hazard Model 2022: Earthquake recurrence derivation from paleoseismic data and probability of detection* (Vol. 2022/32). Lower Hutt (NZ): GNS Science.

Cohen, S. C., & Freymueller, J. T. (1997). Deformation of the Kenai Peninsula, Alaska. *Journal of Geophysical Research: Solid Earth*, 102 (B9), 20479-20487. <https://doi.org/10.1029/97JB01513>

Cross, R. S., & Freymueller, J. T. (2008). Evidence for and implications of a Bering plate based on geodetic measurements from the Aleutians and western Alaska. *Journal of Geophysical Research: Solid Earth*, 113 (B7), B07405. <https://doi.org/10.1029/2007JB005136>

Daly, K. A., Abers, G. A., Mann, M. E., Roecker, S., & Christensen, D. H. (2021). Subduction of an oceanic plateau across southcentral Alaska: High-resolution seismicity. *Journal of Geophysical Research: Solid Earth*, 126 (11), e2021JB022809. <https://doi.org/10.1029/2021JB022809>

Davies, J., Sykes, L., House, L., & Jacob, K. (1981). Shumagin seismic gap, Alaska Peninsula: History of great earthquakes, tectonic setting, and evidence for high seismic potential. *Journal of Geophysical Research: Solid Earth*, 86 (B5), 3821-3855. <https://doi.org/10.1029/JB086iB05p03821>

Drooff, C., & Freymueller, J. T. (2021). New constraints on slip deficit on the Aleutian megathrust and inflation at Mt. Veniaminof, Alaska from repeat GPS measurements. *Geophysical Research Letters*, 48 (4), e2020GL091787. <https://doi.org/10.1029/2020GL091787>

Eberhart-Phillips, D., Christensen, D. H., Brocher, T. M., Hansen, R., Ruppert, N. A., Haeussler, P. J., & Abers, G. A. (2006). Imaging the transition from Aleutian subduction to Yakutat collision in central Alaska, with local earthquakes and active source data. *Journal of Geophysical Research: Solid Earth*, 111 (B11), B11303. <https://doi.org/10.1029/2005JB004240>

Elliott, J., & Freymueller, J. T. (2020). A block model of present-day kinematics of Alaska and western Canada. *Journal of Geophysical Research: Solid Earth*, 125 (7), e2019JB018378. <https://doi.org/10.1029/2019JB018378>

Elliott, J., Freymueller, J. T., & Larsen, C. F. (2013). Active tectonics of the St. Elias orogen, Alaska, observed with GPS measurements. *Journal of Geophysical Research: Solid Earth*, 118 (10), 5625-5642. <https://doi.org/10.1002/jgrb.50341>

Elliott, J. L., Grapenthin, R., Parameswaran, R. M., Xiao, Z., Freymueller, J. T., & Fusso, L. (2022). Cascading rupture of a megathrust. *Science Advances*, 8 (18), eabm4131. <https://doi.org/10.1126/sciadv.abm4131>

- Engelhart, S. E., Horton, B. P., & Dura, T. (2015). Paleoseismology of Sanak Island: Collaborative Research with University of Rhode Island, Rutgers University, and U.S. Geological Survey. *Final Technical Report, USGS External Grants*, 30 pp. [https://earthquake.usgs.gov/cfusion/external\\_grants/research.cfm](https://earthquake.usgs.gov/cfusion/external_grants/research.cfm)
- Estabrook, C. H., & Boyd, T. M. (1992). The Shumagin Islands, Alaska, earthquake of 31 May 1917. *Bulletin of the Seismological Society of America*, 82 (2), 755-773. <https://doi.org/10.1785/BSSA0820020755>
- Estabrook, C. H., Nábělek, J. L., & Lerner-Lam, A. L. (1992). Tectonic model of the Pacific-North American plate boundary in the Gulf of Alaska from broadband analysis of the 1979 St. Elias, Alaska, earthquake and its aftershocks. *Journal of Geophysical Research: Solid Earth*, 97 (B5), 6587-6612. <https://doi.org/10.1029/92JB00131>
- Field, E. H., Arrowsmith, R. J., Biasi, G. P., Bird, P., Dawson, T. E., Felzer, K. R., et al. (2014). Uniform California Earthquake Rupture Forecast, Version 3 (UCERF3) —The time-independent model. *Bulletin of the Seismological Society of America*, 104 (3), 1122-1180. <https://doi.org/10.1785/0120130164>
- Field, E. H., Biasi, G. P., Bird, P., Dawson, T. E., Felzer, K. R., Jackson, D. D., et al. (2013). Uniform California earthquake rupture forecast, version 3 (UCERF3): The time-independent model. *U.S. Geological Survey Open-File Report 2013-1165*, 97 pp. <https://doi.org/10.3133/ofr20131165>
- Field, E. H., Milner, K. R., & Page, M. T. (2020). Generalizing the inversion-based PSHA source model for an interconnected fault system. *Bulletin of the Seismological Society of America*, 111 (1), 371-390. <https://doi.org/10.1785/0120200219>
- Fournier, T. J., & Freymueller, J. T. (2007). Transition from locked to creeping subduction in the Shumagin region, Alaska. *Geophysical Research Letters*, 34 (6), L06303. <https://doi.org/10.1029/2006GL029073>
- Frankel, A., Chen, R., Petersen, M., Moschetti, M., & Sherrod, B. (2015). 2014 Update of the Pacific Northwest portion of the U.S. National Seismic Hazard Maps. *Earthquake Spectra*, 31 (1\_suppl), S131-S148. <https://doi.org/10.1193/111314EQS193M>
- Freymueller, J. T., & Beavan, J. (1999). Absence of strain accumulation in the Western Shumagin Segment of the Alaska Subduction Zone. *Geophysical Research Letters*, 26 (21), 3233-3236. <https://doi.org/10.1029/1999GL008356>
- Freymueller, J. T., Cohen, S. C., & Fletcher, H. J. (2000). Spatial variations in present-day deformation, Kenai Peninsula, Alaska, and their implications. *Journal of Geophysical Research: Solid Earth*, 105 (B4), 8079-8101. <https://doi.org/10.1029/1999JB900388>
- Freymueller, J. T., Suleimani, E. N., & Nicolisky, D. J. (2021). Constraints on the slip distribution of the 1938  $M_W$  8.3 Alaska Peninsula earthquake from tsunami modeling. *Geophysical Research Letters*, 48 (9), e2021GL092812. <https://doi.org/10.1029/2021GL092812>
- Freymueller, J. T., Woodard, H., Cohen, S. C., Cross, R., Elliot, J., Larsen, C. F., et al. (2008). Active deformation processes in Alaska, based on 15 years of GPS measurements. In: J. T. Freymueller, P. J. Haeussler, R. L. Wesson, & G. Ekström (Eds.) *Active Tectonics and Seismic Potential of Alaska: Geophysical Monograph Series 179* (pp. 1-42), Washington, DC: American Geophysical Union. <https://doi.org/10.1029/179GM02>
- GEBCO Compilation Group (2023). GEBCO 2023 Grid. <https://doi:10.5285/f98b053b-0cbc-6c23-e053-6c86abc0af7b>
- Geist, E. L., Childs, J. R., & Scholl, D. W. (1988). The origin of summit basins of the Aleutian Ridge: Implications for block rotation of an arc massif. *Tectonics*, 7 (2), 327-341. <https://doi.org/10.1029/TC007i002p00327>
- Gilpin, L. M. (1995). *Holocene paleoseismicity and coastal tectonics of the Kodiak Islands, Alaska*. Ph.D. dissertation, University of California, Santa Cruz, 358 pp.
- Gilpin, L. M., Carver, G.A., and Hemphill-Haley, E. (1994). Paleoseismicity of the SW extent of the 1964 Alaskan rupture zone, eastern Aleutian arc, Kodiak Island, Alaska. In: D. P. Schwartz & R. S. Yeats (Eds.)

- Proceedings of the workshop on Paleoseismology, 18-22 September 1994, Marshall, California. *U.S. Geological Survey Open-File Report 94-568* (p. 70). <https://doi.org/10.3133/ofr94568>
- Goldfinger, C., Nelson, C. H., Morey, A. E., Johnson, J. E., Patton, J. R., Karabanov, E. B., et al. (2012). Turbidite event history—Methods and implications for Holocene paleoseismicity of the Cascadia subduction zone. *U.S. Geological Survey Professional Paper 1661-F*, 170 pp. <https://doi.org/10.3133/pp1661F>
- Hamilton, S., & Shennan, I. (2005a). Late Holocene great earthquakes and relative sea-level change at Kenai, southern Alaska. *Journal of Quaternary Science*, *20* (2), 95-111. <https://doi.org/10.1002/jqs.903>
- Hamilton, S., & Shennan, I. (2005b). Late Holocene relative sea-level changes and the earthquake deformation cycle around upper Cook Inlet, Alaska. *Quaternary Science Reviews*, *24* (12-13), 1479-1498. <https://doi.org/10.1016/j.quascirev.2004.11.003>
- Hatem, A. E., Reitman, N. G., Briggs, R. W., Gold, R. D., Jobe, J. A. T., & Burgette, R. J. (2022). Western U.S. geologic deformation model for use in the U.S. National Seismic Hazard Model 2023. *Seismological Research Letters*, *93* (6), 3053-3067. <https://doi.org/10.1785/0220220154>
- Hawkes, A. D., Horton, B. P., Nelson, A. R., & Hill, D. F. (2010). The application of intertidal foraminifera to reconstruct coastal subsidence during the giant Cascadia earthquake of AD 1700 in Oregon, USA. *Quaternary International*, *221* (1-2), 116-140. <https://doi.org/10.1016/j.quaint.2009.09.019>
- Hayes, G. P., Moore, G. L., Portner, D. E., Hearne, M., Flamme, H., Furtney, M., & Smoczyk, G. M. (2018). Slab2, a comprehensive subduction zone geometry model. *Science*, *362* (6410), 58-61. <https://doi.org/10.1126/science.aat4723>
- Hutchinson, I., & Crowell, A. L. (2007). Recurrence and Extent of Great Earthquakes in Southern Alaska During the Late Holocene from an Analysis of the Radiocarbon Record of Land-Level Change and Village Abandonment. *Radiocarbon*, *49* (3), 1323-1385. <https://doi.org/10.1017/S0033822200043198>
- Ichinose, G., Somerville, P., Thio, H. K., Graves, R., & O'Connell, D. (2007). Rupture process of the 1964 Prince William Sound, Alaska, earthquake from the combined inversion of seismic, tsunami, and geodetic data. *Journal of Geophysical Research: Solid Earth*, *112* (B7). <https://doi.org/10.1029/2006JB004728>
- Johnson, J. M., & Satake, K. (1993). Source parameters of the 1957 Aleutian earthquake from tsunami waveforms. *Geophysical Research Letters*, *20* (14), 1487-1490. <https://doi.org/10.1029/93GL01217>
- Johnson, J. M., & Satake, K. (1997). Estimation of seismic moment and slip distribution of the April 1, 1946, Aleutian tsunami earthquake. *Journal of Geophysical Research: Solid Earth*, *102* (B6), 11765-11774. <https://doi.org/10.1029/97JB00274>
- Kelsey, H. M., Witter, R. C., Engelhart, S. E., Briggs, R., Nelson, A., Haeussler, P., & Corbett, D. (2015). Beach ridges as paleoseismic indicators of abrupt coastal subsidence during subduction zone earthquakes, and implications for Alaska-Aleutian subduction zone paleoseismology, southeast coast of the Kenai Peninsula, Alaska. *Quaternary Science Reviews*, *113*, 147-158. <https://doi.org/10.1016/j.quascirev.2015.01.006>
- Kogan, M. G., Frolov, D. I., Vasilenko, N. F., Freymueller, J. T., Steblov, G. M., Ekström, G., et al. (2017). Plate coupling and strain in the far western Aleutian arc modeled from GPS data. *Geophysical Research Letters*, *44* (7), 3176-3183. <https://doi.org/10.1002/2017GL072735>
- Lay, T., Kanamori, H., Ammon, C. J., Koper, K. D., Hutko, A. R., Ye, L., et al. (2012). Depth-varying rupture properties of subduction zone megathrust faults. *Journal of Geophysical Research: Solid Earth*, *117* (B4), B0431. <https://doi.org/10.1029/2011JB009133>
- Lay, T., Ye, L., Bai, Y., Cheung, K. F., Kanamori, H., Freymueller, J., et al. (2017). Rupture Along 400 km of the Bering Fracture Zone in the Komandorsky Islands Earthquake (M<sub>W</sub> 7.8) of 17 July 2017. *Geophysical Research Letters*, *44* (24), 12161-12169. <https://doi.org/10.1002/2017GL076148>

- Li, S., Freymueller, J., & McCaffrey, R. (2016). Slow slip events and time-dependent variations in locking beneath Lower Cook Inlet of the Alaska-Aleutian subduction zone. *Journal of Geophysical Research: Solid Earth*, *121* (2), 1060-1079. <https://doi.org/10.1002/2015JB012491>
- Li, S., & Freymueller, J. T. (2018). Spatial variation of slip behavior beneath the Alaska Peninsula along Alaska-Aleutian subduction zone. *Geophysical Research Letters*, *45* (8), 3453-3460. <https://doi.org/10.1002/2017GL076761>
- Liberty, L. M., Finn, S. P., Haeussler, P. J., Pratt, T. L., and Peterson, A. (2013), Megathrust splay faults at the focus of the Prince William Sound asperity, Alaska, *J. Geophys. Res. Solid Earth*, *118*, 5428–5441, doi:10.1002/jgrb.50372.
- Lisowski, M., Savage, J. C., Prescott, W. H., & Gross, W. K. (1988). Absence of strain accumulation in the Shumagin seismic gap, Alaska, 1980–1987. *Journal of Geophysical Research: Solid Earth*, *93* (B7), 7909-7922. <https://doi.org/10.1029/JB093iB07p07909>
- López, A. M. & Okal, E.A. (2006). A seismological reassessment of the source of the 1946 Aleutian ‘tsunami’ earthquake, *Geophysical Journal International*, *165*(3), 835–849. <https://doi.org/10.1111/j.1365-246X.2006.02899.x>
- Mackey, K. G., Fujita, K., Gunbina, L. V., Kovalev, V. N., Imaev, V. S., Koz’min, B. M., & Imaeva, L. P. (1997). Seismicity of the Bering Strait region: Evidence for a Bering block. *Geology*, *25* (11), 979-982. [https://doi.org/10.1130/0091-7613\(1997\)025%3C0979:SOTBSR%3E2.3.CO;2](https://doi.org/10.1130/0091-7613(1997)025%3C0979:SOTBSR%3E2.3.CO;2)
- Mann, D. H., & Crowell, A. L. (1996). A large earthquake occurring 700–800 years ago in Aialik Bay, southern coastal Alaska. *Canadian Journal of Earth Sciences*, *33* (1), 117-126. <https://doi.org/10.1139/e96-012>
- Mann, M. E., Abers, G. A., Daly, K. A., & Christensen, D. H. (2022). Subduction of an oceanic plateau across southcentral Alaska: Scattered-wave imaging. *Journal of Geophysical Research: Solid Earth*, *127* (1), e2021JB022697. <https://doi.org/10.1029/2021JB022697>
- Mariniere, J., Beauval, C., Nocquet, J. M., Chlieh, M., & Yepes, H. (2021). Earthquake recurrence model for the Colombia–Ecuador subduction zone constrained from seismic and geodetic data, Implication for PSHA. *Bulletin of the Seismological Society of America*, *111* (3), 1508-1528. <https://doi.org/10.1785/0120200338>
- McCann, W. R., Nishenko, S. P., Sykes, L. R., & Krause, J. (1979). Seismic gaps and plate tectonics: Seismic potential for major boundaries. *Pure and Applied Geophysics*, *117* (6), 1082-1147. <https://doi.org/10.1007/BF00876211>
- National Research Council. (1997). *Review of Recommendations for Probabilistic Seismic Hazard Analysis: Guidance on Uncertainty and Use of Experts*. Washington, DC: The National Academies Press, 84 pp. <https://doi.org/10.17226/5487>
- Nelson, A. R., Briggs, R. W., Dura, T., Engelhart, S. E., Gelfenbaum, G., Bradley, L. A., et al. (2015). Tsunami recurrence in the eastern Alaska-Aleutian arc: A Holocene stratigraphic record from Chirikof Island, Alaska. *Geosphere*, *11* (4), 1172-1203. <https://doi.org/10.1130/GES01108.1>
- Nelson, A. R., DuRoss, C. B., Witter, R. C., Kelsey, H. M., Engelhart, S. E., Mahan, S. A., et al. (2021). A maximum rupture model for the central and southern Cascadia subduction zone—reassessing ages for coastal evidence of megathrust earthquakes and tsunamis. *Quaternary Science Reviews*, *261* , 106922. <https://doi.org/10.1016/j.quascirev.2021.106922>
- Newberry, J. T., Laclair, D. L., & Fujita, K. (1986). Seismicity and tectonics of the far western Aleutian Islands. *Journal of Geodynamics*, *6* (1-4), 13-32. [https://doi.org/10.1016/0264-3707\(86\)90030-X](https://doi.org/10.1016/0264-3707(86)90030-X)
- Nicolisky, D. J., Freymueller, J. T., Witter, R. C., Suleimani, E. N., & Koehler, R. D. (2016). Evidence for shallow megathrust slip across the Unalaska seismic gap during the great 1957 Andreanof Islands

- earthquake, eastern Aleutian Islands, Alaska. *Geophysical Research Letters*, 43 (19), 10328-310337. <https://doi.org/10.1002/2016GL070704>
- Nishenko, S. P., & Jacob, K. H. (1990). Seismic potential of the Queen Charlotte-Alaska-Aleutian seismic zone. *Journal of Geophysical Research: Solid Earth*, 95 (B3), 2511-2532. <https://doi.org/10.1029/JB095iB03p02511>
- Noda, H. & Lapusta, N. (2013). Stable creeping fault segments can become destructive as a result of dynamic weakening. *Nature* 493 , 518–521. <https://doi.org/10.1038/nature11703>
- Okal, E. A., & Hébert, H. (2007). Far-field simulation of the 1946 Aleutian tsunami. *Geophysical Journal International*, 169 (3), 1229-1238. <https://doi.org/10.1111/j.1365-246X.2007.03375.x>
- Pacheco, J. F., Sykes, L. R., & Scholz, C. H. (1993). Nature of seismic coupling along simple plate boundaries of the subduction type. *Journal of Geophysical Research-Solid Earth*, 98 (B8), 14133-14159. <https://doi.org/10.1029/93JB00349>
- Pagani, M., Johnson, K., & Garcia Pelaez, J. (2021). Modelling subduction sources for probabilistic seismic hazard analysis. *Geological Society, London, Special Publications*, 501 (1), 225-244. <https://doi.org/10.1144/SP501-2019-120>
- Plafker, G. (1969). Tectonics of the March 27, 1964 Alaska earthquake. *U.S. Geological Survey Professional Paper 543-I* , 74 pp. <https://doi.org/10.3133/pp543I>
- Plafker, G., Lajoie, K. R., & Rubin, M. (1992). Determining recurrence intervals of great subduction zone earthquakes in southern Alaska by radiocarbon dating. In: R. E. Taylor, A. Long, & R. Kra (Eds.), *Radiocarbon After Four Decades* (pp. 436-453), New York: Springer. [https://doi.org/10.1007/978-1-4757-4249-7\\_2](https://doi.org/10.1007/978-1-4757-4249-7_2)
- Pulpan, H., & Frohlich, C. (1985). Geometry of the subducted plate near Kodiak Island and Lower Cook Inlet, Alaska, determined from relocated earthquake hypocenters. *Bulletin of the Seismological Society of America*, 75 (3), 791-810. <https://doi.org/10.1785/BSSA0750030791>
- Ross, S. L., Eble, M., Nicolisky, D. J., & Wilson, R. (2023). Tsunami source standardization for hazards mitigation in the United States. *John Wesley Powell Center for Analysis and Synthesis* . Retrieved from <https://www.sciencebase.gov/catalog/item/59a06151e4b038630d030525>
- Ross, S. L., Jones, L. M., Miller, K., Porter, K. A., Wein, A., Wilson, R. I., et al. (2013). SAFRR (Science Application for Risk Reduction) tsunami scenario—Executive summary and introduction. *U.S. Geological Survey Open-File Report 2013-1170-A* , 17 pp. <https://doi.org/10.3133/ofr20131170A>
- Ryan, H. F., & Coleman, P. J. (1992). Composite transform-convergent plate boundaries: Description and discussion. *Marine and Petroleum Geology*, 9 (1), 89-97. [https://doi.org/10.1016/0264-8172\(92\)90006-Z](https://doi.org/10.1016/0264-8172(92)90006-Z)
- Ryan, H. F., Draut, A. E., Keranen, K., & Scholl, D. W. (2012). Influence of the Amlia fracture zone on the evolution of the Aleutian Terrace forearc basin, central Aleutian subduction zone. *Geosphere*, 8 (6), 1254-1273. <https://doi.org/10.1130/GES00815.1>
- Satake, K., & Atwater, B. F. (2007). Long-term perspectives on giant earthquakes and tsunamis at subduction zones. *Annual Review of Earth and Planetary Sciences*, 35 (1), 349-374. <https://doi.org/10.1146/annurev.earth.35.031306.140302>
- Savage, J. C., J. L. Svarc, W. H. Prescott, and W. K. Gross (1998), Deformation across the rupture zone of the 1964 Alaska earthquake 1993–1997, *J. Geophys. Res.*, 103, 21,275–21,283, <https://doi.org/10.1029/98JB02048>.
- Savage, J. C., Lisowski, M., & Prescott, W. H. (1986). Strain accumulation in the Shumagin and Yakataga seismic gaps, Alaska. *Science*, 231 (4738), 585-587. <https://doi.org/10.1126/science.231.4738.585>

- Schmalzle, G. M., McCaffrey, R., & Creager, K. C. (2014). Central Cascadia subduction zone creep. *Geochemistry, Geophysics, Geosystems*, *15* (4), 1515-1532. <https://doi.org/10.1002/2013GC005172>
- Scholz, C. H., & Campos, J. (2012). The seismic coupling of subduction zones revisited. *Journal of Geophysical Research: Solid Earth*, *117* (B5), B05310. <https://doi.org/10.1029/2011JB009003>
- Schwartz, S. Y. (1999). Noncharacteristic behavior and complex recurrence of large subduction zone earthquakes. *Journal of Geophysical Research: Solid Earth*, *104* (B10), 23111-23125. <https://doi.org/10.1029/1999JB900226>
- Shaw, B. E. (2023). Magnitude and slip scaling relations for fault-based seismic hazard. *Bulletin of the Seismological Society of America*, *113* (3), 924-947. <https://doi.org/10.1785/0120220144>
- Shennan, I., Brader, M. D., Barlow, N. L. M., Davies, F. P., Longley, C., & Tunstall, N. (2018). Late Holocene paleoseismology of Shuyak Island, Alaska. *Quaternary Science Reviews*, *201*, 380-395. <https://doi.org/10.1016/j.quascirev.2018.10.028>
- Shennan, I., Bruhn, R., Barlow, N., Good, K., & Hocking, E. (2014). Late Holocene great earthquakes in the eastern part of the Aleutian megathrust. *Quaternary Science Reviews*, *84*, 86-97. <https://doi.org/10.1016/j.quascirev.2013.11.010>
- Shennan, I., Bruhn, R., & Plafker, G. (2009). Multi-segment earthquakes and tsunami potential of the Aleutian megathrust. *Quaternary Science Reviews*, *28* (1-2), 7-13. <https://doi.org/10.1016/j.quascirev.2008.09.016>
- Shennan, I., Garrett, E., & Barlow, N. (2016). Detection limits of tidal-wetland sequences to identify variable rupture modes of megathrust earthquakes. *Quaternary Science Reviews*, *150*, 1-30. <https://doi.org/10.1016/j.quascirev.2016.08.003>
- Small, D. T., & Melgar, D. (2021). Geodetic coupling models as constraints on stochastic earthquake ruptures: An example application to PTHA in Cascadia. *Journal of Geophysical Research: Solid Earth*, *126* (7), e2020JB021149. <https://doi.org/10.1029/2020JB021149>
- Stirling, M., McVerry, G., Gerstenberger, M., Litchfield, N., Van Dissen, R., Berryman, K., et al. (2012). National Seismic Hazard Model for New Zealand: 2010 Update. *Bulletin of the Seismological Society of America*, *102* (4), 1514-1542. <https://doi.org/10.1785/0120110170>
- Suito, H., & Freymueller, J. T. (2009). A viscoelastic and afterslip postseismic deformation model for the 1964 Alaska earthquake. *Journal of Geophysical Research: Solid Earth*, *114* (B11), B11404. <https://doi.org/10.1029/2008JB005954>
- Sykes, L. R. (1971). Aftershock zones of great earthquakes, seismicity gaps, and earthquake prediction for Alaska and the Aleutians. *Journal of Geophysical Research*, *76* (32), 8021-8041. <https://doi.org/10.1029/JB076i032p08021>
- Tanioka, Y., & Gonzalez, F. I. (1998). The Aleutian Earthquake of June 10, 1996 (Mw 7.9) ruptured parts of both the Andreanof and Delarof segments. *Geophysical Research Letters*, *25* (12), 2245-2248. <https://doi.org/10.1029/98GL01578>
- Tape, C., & Lomax, A. (2022). Aftershock regions of Aleutian-Alaska megathrust earthquakes, 1938–2021. *Journal of Geophysical Research: Solid Earth*, *127* (7), e2022JB024336. <https://doi.org/10.1029/2022JB024336>
- Taylor, F. W., Frohlich, C., Lecolle, J., & Strecker, M. (1987). Analysis of partially emerged corals and reef terraces in the central Vanuatu Arc: Comparison of contemporary coseismic and nonseismic with quaternary vertical movements. *Journal of Geophysical Research: Solid Earth*, *92* (B6), 4905-4933. <https://doi.org/10.1029/JB092iB06p04905>

- Tsang, L. L. H., Meltzner, A. J., Hill, E. M., Freymueller, J. T., & Sieh, K. (2015). A paleogeodetic record of variable interseismic rates and megathrust coupling at Simeulue Island, Sumatra. *Geophysical Research Letters*, *42*, 10,585–10,594. <https://doi.org/10.1002/2015GL066366>
- von Huene, R., Klaeschen, D., & Fruehn, J. (1999). Relation between the subducting plate and seismicity associated with the great 1964 Alaska earthquake. *Pure and Applied Geophysics*, *154* (3), 575-591. <https://doi.org/10.1007/s000240050245>
- von Huene, R., Miller, J. J., & Weinrebe, W. (2012). Subducting plate geology in three great earthquake ruptures of the western Alaska margin, Kodiak to Unimak. *Geosphere*, *8* (3), 628-644. <https://doi.org/10.1130/GES00715.1>
- Wang, K. (1995). Coupling of tectonic loading and earthquake fault slips at subduction zones. *Pure and Applied Geophysics*, *145* (3), 537-559. <https://doi.org/10.1007/BF00879588>
- Wech, A. G. (2016). Extending Alaska's plate boundary: Tectonic tremor generated by Yakutat subduction. *Geology*, *44* (7), 587-590. <https://doi.org/10.1130/G37817.1>
- Wesson, R. L., Boyd, O. S., Mueller, C. S., Bufe, C. G., Frankel, A. D., & Petersen, M. D. (2007). Revision of time-independent probabilistic seismic hazard maps for Alaska. *U.S. Geological Survey Open-File Report 2007-1043*, 33 pp. <https://doi.org/10.3133/ofr20071043>
- Working Group on California Earthquake Probabilities (WGCEP) (2003). Earthquake probabilities in the San Francisco Bay region: 2002 to 2031. *U.S. Geological Survey. Open File Report 2003-214*, 235 pp. <https://doi.org/10.3133/ofr03214>
- Witter, R., Briggs, R., Engelhart, S. E., Gelfenbaum, G., Koehler, R. D., Nelson, A., et al. (2019). Evidence for frequent, large tsunamis spanning locked and creeping parts of the Aleutian megathrust. *GSA Bulletin*, *131* (5-6), 707-729. <https://doi.org/10.1130/B32031.1>
- Witter, R. C., Briggs, R. W., Engelhart, S. E., Gelfenbaum, G., Koehler, R. D., & Barnhart, W. D. (2014). Little late Holocene strain accumulation and release on the Aleutian megathrust below the Shumagin Islands, Alaska. *Geophysical Research Letters*, *41* (7), 2359-2367. <https://doi.org/10.1002/2014GL059393>
- Witter, R. C., Carver, G. A., Briggs, R. W., Gelfenbaum, G., Koehler, R. D., La Selle, S., et al. (2016). Unusually large tsunamis frequent a currently creeping part of the Aleutian megathrust. *Geophysical Research Letters*, *43* (1), 76-84. <https://doi.org/10.1002/2015GL066083>
- Worthington, L. L., Gulick, S. P. S., & Pavlis, T. L. (2008). Identifying active structures in the Kayak Island and Pamplona zones: Implications for offshore tectonics of the Yakutat microplate, Gulf of Alaska. In: J. T. Freymueller, P. J. Haeussler, R. L. Wesson, & G. Ekstrom (Eds.) *Active Tectonics and Seismic Potential of Alaska: Geophysical Monograph Series 179* (pp. 257-268), Washington, DC: American Geophysical Union. <https://doi.org/10.1029/179GM14>
- Worthington, L. L., Van Avendonk, H. J. A., Gulick, S. P. S., Christeson, G. L., & Pavlis, T. L. (2012). Crustal structure of the Yakutat terrane and the evolution of subduction and collision in southern Alaska. *Journal of Geophysical Research: Solid Earth*, *117* (B1), B01102. <https://doi.org/10.1029/2011JB008493>
- Xiao, Z., Freymueller, J. T., Grapenthin, R., Elliott, J., Drooff, C., & Fusso, L. (2021). The deep Shumagin gap filled: Kinematic rupture model and slip budget analysis of the 2020 Mw 7.8 Simeonof earthquake constrained by GNSS, global seismic waveforms, and floating InSAR. *Earth and Planetary Science Letters*, *576*, 117241, <https://doi.org/10.1016/j.epsl.2021.117241>
- Xue, X., & Freymueller, J. T. (2020). A 25-year history of volcano magma supply in the east central Aleutian arc, Alaska. *Geophysical Research Letters*, *47* (15), e2020GL088388. <https://doi.org/10.1029/2020GL088388>
- Ye, L., Bai, Y., Si, D., Lay, T., Cheung, K. F., & Kanamori, H. (2022). Rupture model for the 29 July 2021 Mw 8.2 Chignik, Alaska earthquake constrained by seismic, geodetic, and tsunami observations. *Journal of*

Ye, S., Flueh, E. R., Klaeschen, D., & von Huene, R. (1997). Crustal structure along the EDGE transect beneath the Kodiak shelf off Alaska derived from OBH seismic refraction data. *Geophysical Journal International*, 130 (2), 283-302. <https://doi.org/10.1111/j.1365-246X.1997.tb05648.x>

Zhao, B., Burgmann, R., Wang, D., Zhang, J., Yu, J., & Li, Q. (2022). Aseismic slip and recent ruptures of persistent asperities along the Alaska-Aleutian subduction zone. *Nature Communications*, 13, 3098. <https://doi.org/10.1038/s41467-022-30883-7>

**Tables**

Table 1

Geologic recurrence data

Table 1. Geologic recurrence intervals

Fault Section	Paleoearthquake timing <sup>a</sup>	Mean paleoearthquake recurrence <sup>b</sup>	Mean paleoearthquake recurrence uncertainty (± years)	Paleotsunami timing	Mean paleotsunami recurrence (years)	Mean paleotsunami recurrence uncertainty (± years)	References for paleoearthquakes <sup>c</sup>	References for paleotsunamis <sup>d</sup>
Yakataga	~870 BP, ~1440 BP	1513/2 = 757 (open interval)	264	n/d	n/d	n/d	Sh09, modified by Sh14	n/d
Prince William Sound	1964 CE, ~870 BP, ~1440 BP, ~2050 BP, ~2615 BP, ~3130 BP, ~3550 BP	3564/6 = 594 (closed interval)	+15 / -18	n/d	n/d	n/d	CP08; Sh14	n/d
Kenai	1964 CE, ~265 BP, ~867 BP	881/2 = 441 (closed interval)	228	n/d	n/d	n/d	CP08; Sh14; K15	n/d
Barren Islands	n/d	441 inferred from neighboring Kenai section	222	n/d	n/d	n/d	n/d	n/d
Kodiak	1964 CE, 1788 CE, ~500 BP, ~870 BP, ~1500 BP	1514/4 = 379 (closed interval)	188	n/d	n/d	n/d	CP08; Sh14	n/d
Semidi	1788 AD, ~500 BP, ~650 BP, ~870 BP, ~1050 BP	888/4 = 222 (closed interval)	76	13 since 3.5 ka	180-270, mean = 225	45	B14	N15
Shumagin	>3,400 years	>3,400	n/d	n/d	n/d	n/d	W14	n/d
Sanak	n/d	n/d	n/d	1946, gap to 2ka, then 4 sands ~2 ka to ~4 ka	~4ka to 1946 is 3996/4 = 999 (closed interval)	665	n/d	En15
Fox Islands	n/d	n/d	n/d	1957, and 6-8 total since ~2 ka	164-257, mean=210	47	n/d	W19
Andreanof	n/d	n/d	n/d	n/d	n/d	n/d	n/d	n/d
Adak	n/d	n/d	n/d	n/d	n/d	n/d	n/d	n/d
Amchitka	n/d	n/d	n/d	n/d	n/d	n/d	n/d	n/d
Attu	n/d	n/d	n/d	n/d	n/d	n/d	n/d	n/d
Komandorski	n/d	n/d	n/d	n/d	n/d	n/d	n/d	/d

Notes. <sup>a</sup> n/d = no data <sup>b</sup> +73 years (correction from CE1950 to CE2023) for BP convention for open interval; all others closed. <sup>c</sup> References: Sh09 = Shennan et al., 2009; Sh14 = Shennan et al., 2014; CP08 = Carver and Plafker, 2008; K15 = Kelsey et al., 2015; B14 = Briggs et al., 2014; W14 = Witter et al., 2014. <sup>d</sup> References: N15 = Nelson et al., 2015; En15 = Engelhart et al., 2015; W16 = Witter et al., 2016; W19 = Witter et al., 2019

Table 2

Geodetic recurrence data

Table 2. Geodetic recurrence intervals

Section	Geodetic area (km <sup>2</sup> )	Pac-Arc Obs (mm/yr)	Coupling (%)	M <sub>w</sub> 1 (3.9 <sup>a</sup> )	M <sub>w</sub> 2 (4.0 <sup>a</sup> )	M <sub>w</sub> 3 (4.1 <sup>a</sup> )	M <sub>w</sub> 1, slip per event <sup>b</sup> (m)	M <sub>w</sub> 2, slip per event <sup>b</sup> (m)	M <sub>w</sub> 3, slip per event <sup>b</sup> (m)	Recurrence, M <sub>w</sub> 1 (years)	Recurrence, M <sub>w</sub> 2 (years)	Recurrence, M <sub>w</sub> 3 (years)
Yakataga	4161	57	30	7.52	7.62	7.72	1.7	2.4	3.4	100	141	199
Prince William Sound	88177	59	100	8.85	8.95	9.05	7.9	11.1	15.7	133	188	266
Kenai	23907	60	100	8.28	8.38	8.48	4.1	5.8	8.2	65	92	130
Barren Islands	6871	61	50	7.74	7.84	7.94	2.2	3.1	4.4	67	94	133
Kodiak	48430	63	100	8.59	8.69	8.79	5.8	8.2	11.6	88	125	176
Semidi	23460	66	70	8.27	8.37	8.47	4.1	5.7	8.1	85	120	170
Shumagin	17906	68	30	8.15	8.25	8.35	3.5	5.0	7.1	169	238	337
Sanak	16766	70	2	8.12	8.22	8.32	3.4	4.8	6.8	2381	3363	4750
Fox Islands	17133	72	93	8.13	8.23	8.33	3.5	4.9	6.9	50	70	99
Andreanof	15759	75	25	8.10	8.20	8.30	3.3	4.7	6.6	190	268	379
Adak	21314	70	100	8.23	8.33	8.43	3.9	5.5	7.7	57	80	113
Amchitka	32877	68	50	8.42	8.52	8.62	4.8	6.8	9.6	148	209	295
Attu	42113	65	62	8.52	8.62	8.72	5.4	7.7	10.8	231	326	460
Komandorski	16100	38	100	8.11	8.21	8.31	3.4	4.7	6.7	88	125	176

Notes. <sup>a</sup> C value from Shaw (2023). <sup>b</sup> Implied slip from Shaw (2023).